Anais da Academia Brasileira de Ciências (2016) 88(4): 2167-2193
(Annals of the Brazilian Academy of Sciences)
Printed version ISSN 0001-3765 / Online version ISSN 1678-2690
http://dx.doi.org/10.1590/0001-3765201620150088
www.scielo.br/aabc

Paralavas in the Cretaceous Paraná volcanic province, Brazil – A genetic interpretation of the volcanic rocks containing phenocrysts and glass

SÉRGIO B. BAGGIO[1], LÉO A. HARTMANN[1] and ROSA M.S. BELLO[2]

[1]Instituto de Geociências, Universidade Federal do Rio Grande do Sul, Avenida Bento Gonçalves, 9500, Agronomia, 91501-970 Porto Alegre, RS, Brazil
[2]Instituto de Geociências, Universidade de São Paulo, Rua do Lago, 562, 05508-080 São Paulo, SP, Brazil

Manuscript received on February 10, 2015; accepted for publication on July 5, 2016

ABSTRACT

The occurrences of glassy rocks containing long and curved phenocrysts in the Paraná volcanic province, South America, are here interpreted as paralavas. The large number of thin (0.1-0.5 m) dikes and sills of glassy volcanic rocks with hopper, hollow or curved, large crystals of clinopyroxene (up to 10 cm), plagioclase (up to 1 cm), magnetite and apatite are contained in the core of thick (>70 m) pahoehoe flows. They are strongly concentrated in the state of Paraná, coincident with the presence of the large number of dikes in the Ponta Grossa arch. These rocks were previously defined as pegmatites, although other names have also been used. A paralava is here interpreted as the product of melting of basaltic rocks following varied, successive processes of sill emplacement in high-kerogen bituminous shale and ascent of the resultant methane. As the gas reached the lower portion of the most recent lava flow of the volcanic pile, the methane reacted with the silicate and oxide minerals of the host volcanic rock (1,000 ºC) and thus elevated the local temperature to 1,600 ºC. The affected area of host rock remelted (possibly 75 wt.%) and injected buoyantly the central and upper portion of the core. This methane-related mechanism explains the evidence found in the paralavas from this volcanic province, one of the largest in the continents.

Key words: Paralava, Paraná volcanic province, pyrometamorphism, remelting, metal remobilization.

INTRODUCTION

In the Paraná volcanic province (Figure 1), there are occurrences of paralavas that are genetically related to remelting of the holocrystalline host rock at 1,600 ºC. These rocks were previously denominated pegmatites or segregation sheets and occur in all continental volcanic provinces and plutonic rocks of basaltic composition from many provinces. The formation of these rocks is usually ascribed to magmatic processes that involve crystal fractionation and the filter-pressing ascent of the fractionated liquid to form dikes and sills within the mother flow or intrusion. The universal presence of long, thin, hollow crystals in a glassy matrix is a common description of paralavas that resulted from quenching during pyrometamorphism (Grapes et al. 2013).

The presence of the voluminous, glassy matrix in coarse-grained basalt is a recurring feature in large volcanic provinces but is still a paradox that remains to be solved. Several questions arise and

Correspondence to: Sérgio B. Baggio
E-mail: sergio.baggio@ufrgs.br

remain unanswered from the presence of quenched paralavas in thick basalt flows: (1) Processes that caused a strong, local increase in temperature, so the nearly solid basalt remelted; (2) The chemical fractionation of the paralava as compared to the host basalt; (3) The rise of the newly-formed magma through the solid, hot basalt; (4) The quenching of the ascending liquid due to strong thermal disequilibrium with the host basalt; and (5) The initial, strongly reduced composition of the paralava. We presently address all these questions and interpret them in a unified genetic model.

In occurrences of gabbroic pegmatites from Skaergaard (Larsen et al. 1992), fluids are dominated by H_2O, CO_2 and CH_4 as inclusions in plagioclase, quartz and apatite. The source of the carbon component was attributed to assimilation of sedimentary blocks from the volcanoclastic sequence, but the hypothesis of magmatic origin of carbon in silicate glass inclusions (MORB type magma) was not ruled out. Although this evaluation is close to the actual process involved in the formation of these rocks, it is likely that the processes involved in their origin are variable, particularly the types of fluids present. All evaluations attribute the mobility of the fractionated fluid to the presence of gases, but the provenance of the gases is considered the degassing of the host magma (Puffer and Horter 1993). The evidence evaluated thus far relies on a single source of energy, namely the heat liberated from the cooling magma. An additional source of energy seems necessary to remelt the host basalt, adding complexity to the processes involved. We propose a unified description of processes, including field evidence and the interpretation of geochemistry in a scenario of methane generation in the basin and its ascent and reaction in the hot, solid lava. We found the evidence in outcrops of the Paraná volcanic province where reactive relationships are present between the host basalt and the surrounding paralava. We describe here this evidence from Francisco Beltrão (near the depocenter of the Paraná Basin), including field relationships, petrography, rock geochemistry, electron microprobe and fluid inclusions in quartz and plagioclase. The origin of these rocks constitutes a significant problem not yet solved in igneous petrology. The copper enrichment in the paralavas gives economic significance to these rocks.

MATERIALS AND METHODS

The study of paralavas in the Paraná volcanic province derived from several years of research of hydrothermal mineralization hosted in volcanic rocks (e.g., Duarte et al. 2009, 2011, Hartmann et al. 2012a, b, Rosenstengel and Hartmann 2012) and sand injectite structures (Hartmann et al. 2013). Field studies for the present study focused in two areas (Figure 1) that provided significant evidence for the genetic interpretation. The first area is located in southwestern Paraná State that was previously described by Wildner et al. (2006); their samples AS, KN and WW are used here. Dalba quarry in the municipality of Francisco Beltrão is within this area. Samples P1b, R2Pb are from the host basalt, while PD1, P2p, P3p and P4 are from the paralavas in this quarry. Sample PD1 was collected for fluid inclusions and contains samples P2p and P3p, while P4 is a green core collected for XRD. The second area is the Rochasul quarry, located in the town of Jardim, west-central Mato Grosso do Sul State, where sample MS36 was collected.

The methodology included evaluation and description of paralava outcrops indicating the elevation and geographical coordinates (Garmin GPS). The sampled host volcanic rocks (n = 13) and paralavas (n = 14) were analyzed for major and trace elements in the ACME laboratories, Canada. Thin sections from these samples were prepared at UFRGS and at the Geological Survey of Brazil (CPRM/PA). X-ray diffraction (n = 1) was performed in the laboratories of

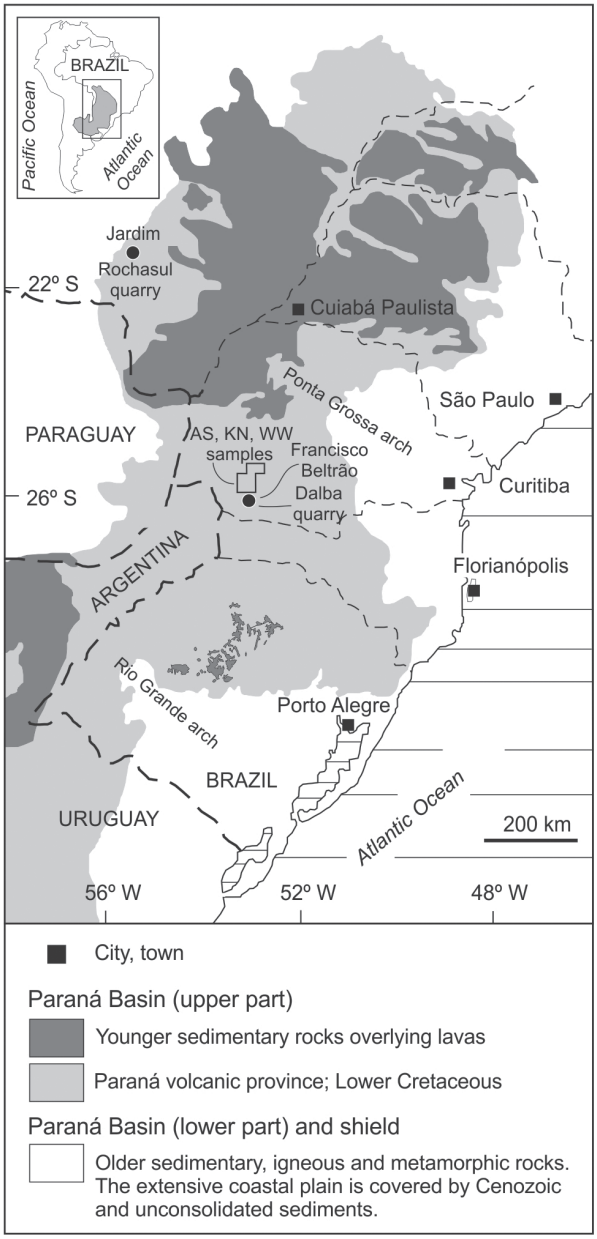

Figure 1 - Geological map of the southeastern portion of South America, highlighting the Paraná Basin, Paraná volcanic province (light grey). Younger sedimentary rocks overlying lavas (dark gray) are the Bauru Group sedimentary rocks (Paraná, São Paulo and Mato Grosso do Sul states), Tupanciretã Formation (Rio Grande do Sul state), Acaray Formation in Paraguay and Mariano Boedo Formation in Argentina. Older sedimentary, igneous and metamorphic rocks and an extensive coastal plain covered by Cenozoic sediments are indicated (white area). The study areas of paralavas are located in the Dalba quarry, Francisco Beltrão (PR) and the Rochasul quarry, Jardim (MS). The indicated area in the Paraná state is related to the samples initialled with AS, KN and WW from CPRM. Map modified from Peate et al. (1992).

UFRGS with a Siemens Bruker-AXS D5000 with 2θ goniometer, radiation Kαl copper tube. Electron microprobe analyses and backscattered electron images were obtained for magnetite-ilmenite, augite-pigeonite and feldspar with a Cameca SX-100 equipment housed at the Institut für Mineralogie und Kristallchemie, Stuttgart University, Germany. The routine measurement protocols used were 15 kV accelerating voltage, 15 nA beam current and a beam size approximately 1 μm. The fluid inclusions study was undertaken at the Núcleo de Apoio à Pesquisa Geoanalítica, Instituto de Geociências, Universidade de São Paulo (Geoanalítica - USP Facility). Four double-polished thin sections were prepared from sample PD1, suitable for fluid inclusions analyses. During petrographic description using a microscope Leitz Wetzlar, the fluid inclusions were assessed for their characterization, distribution and mode of occurrence to identify their possible origin (primary, secondary or pseudo-secondary), and also for the selection of the best fields for microthermometric analysis. The microthermometry of fluid inclusions was carried out in a CHAIXMECA MTM 85 heating and freezing stage calibrated with chemical compounds of Merck MSP for temperatures higher than 40 °C. The calibration also used synthetic standard Syn Flinc (Synthetic Fluid Inclusions). At -56.6 °C, the composition of standard 1 was 75 mol % H_2O and 25 mol % CO_2. At -21.2 °C, the standard 2 has Eutectic composition of H_2O + NaCl system with 23.2 wt.% NaCl. At -10.7 °C, Standard 3 had eutectic composition of H_2O + KCl system with 19.65 wt.% KCl. At 0 °C and 374.1 °C, the standard 4 was composed of pure water (triple point and critical point, respectively). The standard 5, transition of α quartz to β quartz, was used at 573.0 °C.

Information processing used freeware GCDKit (http://www.gcdkit.org/) for the chemical analyses, DIFFRAC^{PLUS} software for X-ray diffraction (standards of PDF2 database) and Microsoft

Excel worksheet CalcMin (Brandelik 2009) for EPMA data. Interpretations with the determination of fluid inclusions salinity were performed by thermodynamic equations inserted into the software FLUIDS (Bakker 2003). CorelDraw software was used for preparation of figures.

GEOLOGY

The largest number of occurrences of paralavas described in the Paraná volcanic province (n = 38) is located in southwestern Paraná state, previously described as pegmatites (Arioli 2008). Fewer occurrences are known in other portions of the province. The paralavas occur mostly in thick (~70 m) lava flows and usually form small (some 0.1-2.0 m thick, most 1-10 m and a few reaching 100 m in length). They form vertical, inclined or horizontal bodies, including stockworks. The contacts of the intrusive bodies may be sharp but are mostly gradational with the host rocks.

Different names have been used to describe these rocks, most commonly pegmatite (Table I). But the common presence of glass in the groundmass (intersertal texture) precludes the use of the word pegmatite for classification. The presence of long (10 cm), curved, skeletal and hollow crystals immersed in glass requires quenching of the lava. Paralava occurrences have been described in basalt, basaltic andesite and andesite. In this study, we refer to the host rocks as basaltic rocks. The study by Wildner et al. (2006) indicates the presence of 2.5 vol.% silicic rocks in the Paraná volcanic province (e.g., rhyodacite, rhyolite, latite, quartz latite, dacite). However, paralavas have not been described in these rocks. Overall, field relationships of the paralavas are comparable to the description of segregation sheets in the Holyoke flood-basalt flow in the Hartford Basin, Connecticut (Philpotts et al. 1996). Similarly, paralavas in the Paraná volcanic province were generated in the lower third of the flow core and occur only in intrusions in thick lava flows displaying vertical cooling joints (Figure 2a, b). This seems a requirement for the formation of the paralavas. Rapid cooling in thinner flows precludes the formation of significant volumes of paralavas.

There are no occurrences of injected paralavas into the columnar jointing of the host basalt, suggesting that the formation of paralavas was earlier (higher temperature) than the columnar joints. The contacts between the paralavas and host basalt are locally sharp but mostly gradational against a coarse-grained, holocrystalline host basalt. Also, the paralavas do not crosscut the lower or upper contact of the flow and remain confined to the flow.

For the full understanding of the genesis of the paralavas, we examine the sedimentary rocks of the Paraná Basin below the Paraná volcanic province. These rocks are composed mostly by fine to medium-grained sandstones with some siltites, and minor limestones. However, the Ponta Grossa

TABLE I
Names commonly used to classify the volcanic rocks containing phenocrysts and glass in continental volcanic and plutonic basaltic host rocks.

Name	Host rock	Reference
Pegmatite	North Mountain basalt, Nova Scotia Canada	Walker (1953), Greenough and Dostal (1992b)
Pegmatitic segregation vein	Flood basalt	Puffer and Horter (1993)
Pegmatitic segregation sheet	Flood basalt flow	Philpotts et al. (1996)
Pegmatoid gabbro	Basalt, Serra Geral Group	Vasconcellos et al. (2001)
Mafic pegmatite	North Mountain basalt, Nova Scotia Canada	Kontak et al. (2002)
Basic pegmatite	Basalt, Serra Geral Group	Arioli (2008), Silva (2011), Ferreira (2011), Ferreira et al. (2014)
Paralava	Flood basalt and intrusives	This work

Formation (states of Paraná and São Paulo) and the Irati Formation (entire basin) have thick layers of bituminous shales (e.g., Goulart and Jardim 1982). For example, "the Irati Formation, a well-known unit for its oil-prone rocks …, extends almost throughout the entire Paraná Basin. It has an average thickness of 40 m, with peaks of about 70 m..." (Holz et al. 2010). Permian sequences (e.g., Irati Formation) of the Paraná Basin are well represented in the underburden of the Paraná volcanic province in the Rochasul quarry and in the western border of the basin (e.g., Simas et al. 2012, their Figure 1). An example along the eastern border is the description of a drill core near Torres, Rio Grande do Sul (Aborrage and Lopes 1986). At 600 m depth, the core displays 35 m of dark siltites and clayey limestones of the Permian Irati Formation. It is most relevant for the origin of the paralavas that the Irati Formation contains pyrobituminous shales, from which kerogen is extracted commercially by PETROBRAS in São Mateus do Sul (Paraná).

Kerogen (particularly type III) is known to liberate large volumes of methane when intensely heated (Grapes 2011). Twenty-six occurrences of oil in the eolian sandstones near the top of the Paraná Basin in the state of São Paulo had their formation attributed to the intrusion of diabase sills into the black shales of the Irati Formation deeper in the basin (Araújo et al. 2004). As indicated by Aarnes et al. (2010), oil is formed in bituminous shales at a larger distance from the sill and methane is formed closer to the sill contact during the same pyrometamorphic event.

The lower Taquaral Member of the Irati Formation comprises siltstones and gray to black mudstones, and the upper Assistência Member has organic-rich mudstones and shales interbedded with limestones (Holz et al. 2010). The upper Assistência Member is rich in total organic carbon (TOC = 10-25 %; e.g., high in the Lauro Müller region, TOC = 20%). This high-TOC kerogen is known to crack into 95% methane when subjected to temperature >200 °C. Several other formations in the basin also contain black shales. For example, the Serra Alta Formation overlies the Irati Formation and also contains marine shales that contributed to the kerogen budget for methane generation during basalt sill injection. In the Ponta Grossa Formation, TOC seems to be lower, between 0.1-0.6% (Goulart and Jardim 1982).

The host basalts of paralavas in the province are holocrystalline, fine to medium-grained. In the Dalba quarry, the thick basaltic flow has paralava intrusions. Both paralavas and host basalt are cut by the cooling joints indicating that the formation of paralavas was prior to the formation of cooling structures of the volcanic flow. The geological relationships between the host basalt and the paralavas exhibit reaction rims (Figure 2c, d) that are distinct in the field, in petrography and in chemical composition. The reaction rims include a green core and two intervening light and dark grey portions close to the host basalt. The light portion has mostly plagioclase and evolves gradually into a dark grey portion with opaque minerals, plagioclase and pyroxene. The constitution of the green core is mostly celadonite, as determined by x-ray diffraction. However, Arioli (2008) described these portions as dark glass containing about 5 wt.% H_2O. The alteration of glass into celadonite is a well known volcanic process. The largest body of paralavas observed in the Paraná volcanic province occurs in the Rochasul quarry (Figure 2e, f). The exposed dimensions are approximately 20 m in thickness by 200 m in length (Brückmann et al. 2013). The paralavas have typical long and curved clinopyroxene up to 10 cm long. The quarry is entire taken by the paralava without exposure of the host rock. The host rock is interpreted as a sedimentary formation, because the geological contact of the first basalt flow of the Paraná volcanic province, in direct contact with an eolian sandstone of the Botucatu Formation, occurs in a higher topographic

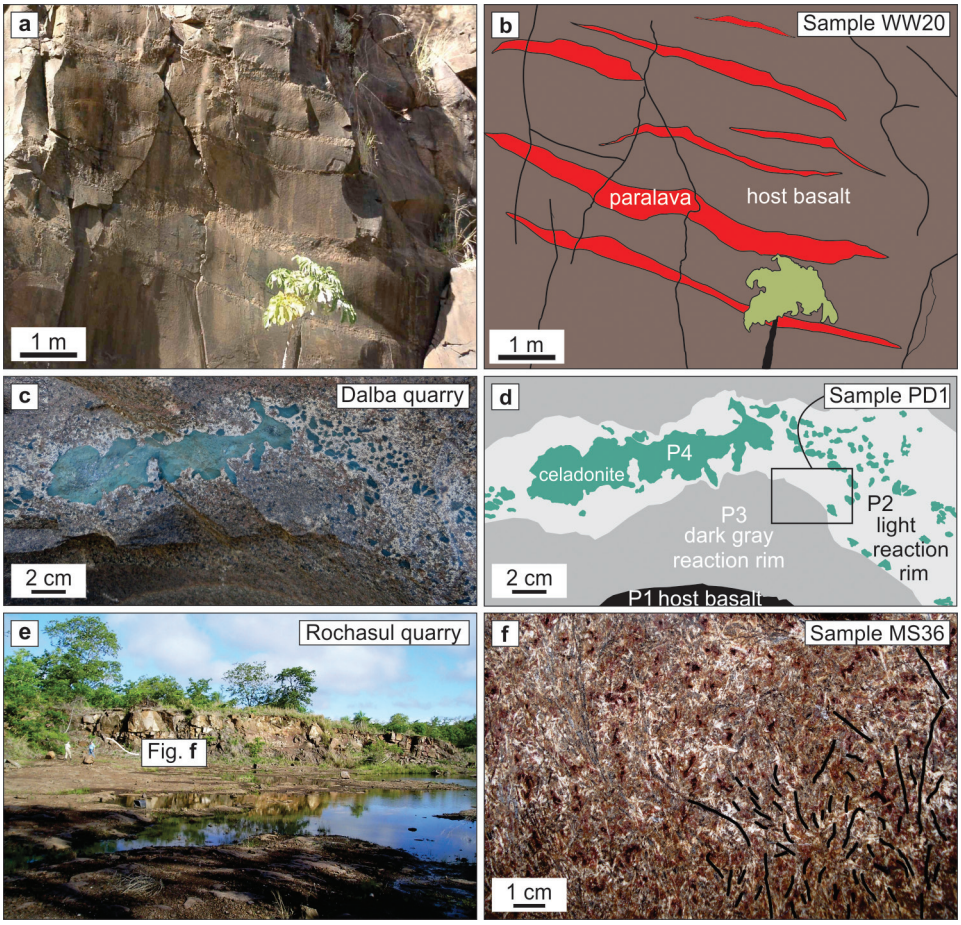

Figure 2 - Field photos of paralava outcrops in the Paraná volcanic province. **a)** Outcrop in northwestern Paraná state showing the paralava sills and the host basalt. **b)** Schematic drawing of Figure 2**a**. **c)** Paralavas from the Dalba quarry, Francisco Beltrão, PR, showing celadonite (dark green core), the dark and light reaction rims and the host basalt. **d)** Schematic drawing of Figure 2**c** with emphasis on the relationship between the contact of the host basalt (sample P1) and the paralava (Samples P2, P3 and P4). **e)** Northern portion of the Rochasul quarry in Jardim, MS, with continuous exposures of paralavas (Sample MS 36). **f)** Detail of paralava in the Rochasul quarry (MS36) highlighting the rock texture and size of the long, curved crystals of clinopyroxene. Clinopyroxene crystals highlighted in small square area.

level along the BR267 highway, eight kilometers distant from the quarry.

RESULTS

PETROGRAPHIC DESCRIPTION

The host basalt is a mesocratic rock, greenish gray, fine grain size. The mineralogical composition (Figure 3) is approximately 48 vol.% plagioclase (mainly labradorite), ~ 26% clinopyroxene (augite and pigeonite), ~16% opaque minerals (magnetite and ilmenite) and ~10% clay minerals (smectite and celadonite). Plagioclase forms elongated crystals (≤0.3 mm) subhedral to euhedral with intergranular texture, whereas the clinopyroxene and opaque minerals occupy the interstices. Plagioclase crystals show corroded borders in direct contact with the smectite or celadonite and no rim alteration in contact with clinopyroxene and opaque minerals. Clinopyroxene forms subhedral to anhedral crystals (0.2-0.3 mm) and has poikilitic inclusions of opaque minerals. Clinopyroxene is

commonly fractured and altered to clay minerals. Opaque minerals range in size from 0.2 to ≤0.5 mm, and may be euhedral (lozenge to hexagonal) or spherical and even anhedral with rim alteration to red iron oxide (hematite). This alteration occurs along fractures and neighboring crystals. Texture varies from subophitic to ophitic. The opaque minerals are euhedral (hexagonal or rectangular), ~0.3 mm in size, mostly without rim alteration. Olivine and apatite occur as accessory minerals in the host rocks.

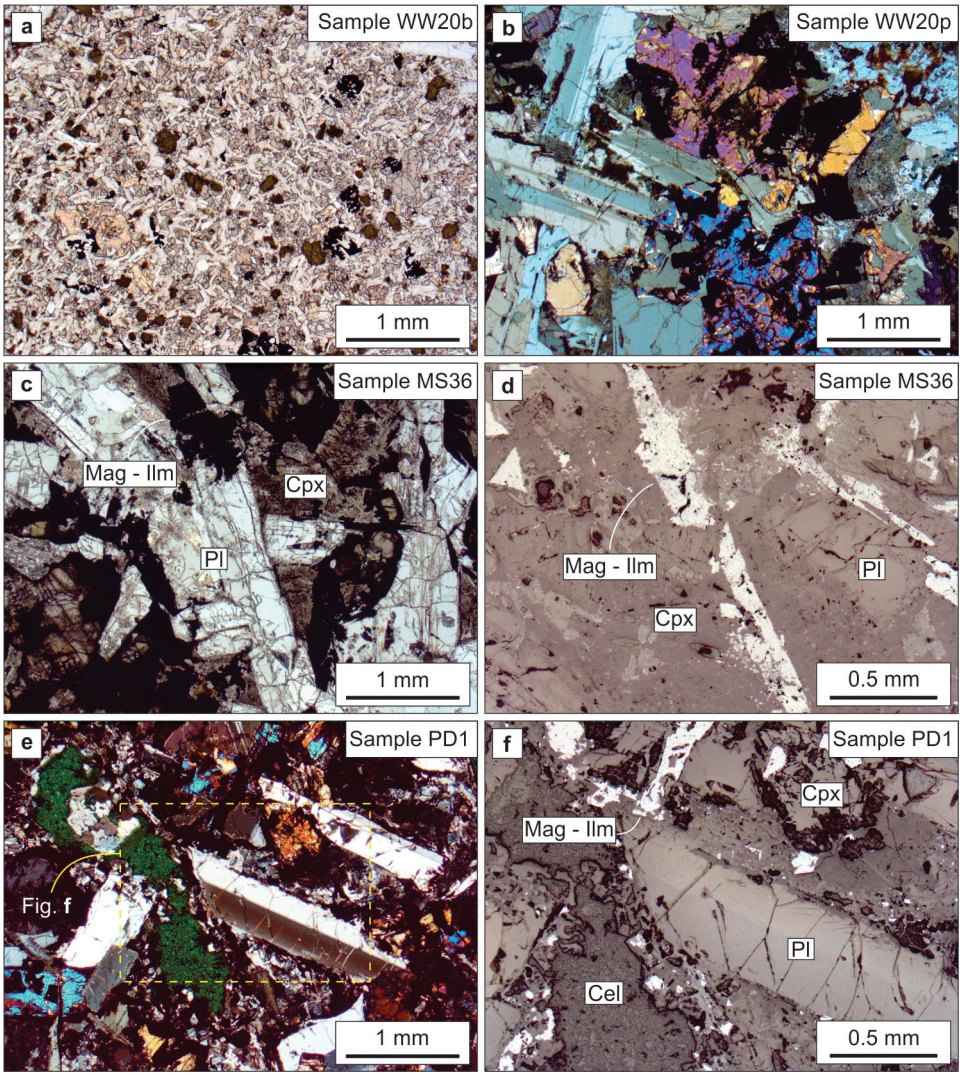

Figure 3 - Photomicrographs of paralavas. **a)** Sample WW20b showing the texture of the host basalt. Plane polarized light. **b)** Sample WW20p showing the phenocrysts of clinopyroxene, plagioclase and opaque minerals in the paralava. Cross polarized light. **c)** Sample MS36 showing the texture of the paralava with crystals of plagioclase, clinopyroxene and magnetite-ilmenite. Plane polarized light. **d)** Sample MS36 showing the relationships between phenocrysts of plagioclase, clinopyroxene and magnetite-ilmenite (reflected light). **e)** Sample PD1 showing the paralava with phenocrysts of plagioclase and smaller crystals of clinopyroxene and areas with celadonite. Plane polarized light. **f)** Sample PD1 showing the relationships between phenocrysts of plagioclase, clinopyroxene and magnetite-ilmenite and areas with celadonite, in reflected light.

The paralavas comprise either horizontal or vertical thin bodies, in some cases forming a stockwork interconnected by veins. In the Dalba quarry (sample PD1), dark and light reaction rims are observed. The mineralogical composition of the dark reaction rim is similar to the host basalt with 45 vol.% plagioclase, ~20% clinopyroxene, ~22% opaque minerals, ~10% clay minerals (smectite and celadonite) and ~3% accessory minerals (apatite and quartz), in addition to traces of carbonates. The opaque minerals (0.1 to 0.2 mm long) are concentrated in the matrix and also in the surrounding pockets of celadonite. Phenocrysts of opaque minerals with anhedral and also skeletal habit show alteration to red iron oxide (hematite). Plagioclase occurs in three distinct habits. The most significant is made up of very fine grained, anhedral crystals associated with quartz that forms a cryptocrystalline matrix in the crystal interstices. This mass of plagioclase is common around the blobs of celadonite. The second plagioclase habit has elongated crystals embedded in the matrix (0.1 to 0.2 mm, whereas the third corresponds to fractured phenocrysts immersed in the matrix. The clinopyroxene (0.1 to 0.2 mm long) is associated with plagioclase and opaque minerals, and occurs also as sparse phenocrysts showing intense fracturing. The celadonite is also scattered in the rock. The mineralogy of the light reaction rim of the paralava (Figure 3) comprises ~ 50 wt.% plagioclase (mainly andesine), ~23% of clinopyroxene (augite), ~20% opaque minerals (magnetite and ilmenite), ~5% celadonite, <1% native copper and traces of apatite and quartz. This mineral assemblage has typically phenocrysts of plagioclase, clinopyroxene and opaque minerals larger than 0.5 mm. The predominant textures are sub-ophitic, ophitic and intersertal. Plagioclase is elongated with the major axis longer than 1 mm; the mineral does not show reaction rims. The clinopyroxene crystals are intensely fractured, whereas the opaque minerals are characterized by a skeletal habit. Apatite is an accessory mineral and stands out in the paralavas for a higher volume (greater than the host basalts), by the needle shape or hexagonal shape in basal (001) sections. Celadonite occurs in green pockets, and veins of celadonite link these pockets with fractures and in many cases cross the fractures of crystals to interconnect with other pockets of celadonite. The native copper mineralization in the paralava (Figure 4) occurs commonly associated with this reaction rim, filling millimetric cavities in association with smectite or celadonite (Figure 4a, b, c). Native copper may be also associated with the clinopyroxene (Figure 4d, e, f). The copper content of the light grey reaction rim is 600 ppm, although the analyzed sample did not have visible metal. The copper content may vary to higher contents due to the nugget effect.

X-RAY DIFFRACTION

The preparation of sample P4 included scraping, separation and concentration of the green core material. The mineralogical determination was performed by the whole rock, X-ray diffraction powder method in the scan range (2θ) from 2° to 72°. The evaluation of these results was based on the peak intensity and the interplanar distances. The main peak intensity had interplanar distances of 9.97 Å, 4.53 Å, 4.35 Å, 3.63 Å, 3.08 Å, 2.57 Å, 2.40 Å e 1.51 Å which identifies celadonite. Other peaks confirmed the presence of plagioclase, quartz and calcite.

ROCK GEOCHEMISTRY

The evaluation of the geochemistry of paralavas requires the understanding of the geochemistry of the host basalts, because they occur only in thick flows (>70 m). The presence of reaction rims between the host basalt and the paralavas in the Dalba quarry motivated us to analyze the reaction rims. In the present evaluation, we make a comparison between the geochemistry of the host basalt and the paralavas. The chemical analyses are

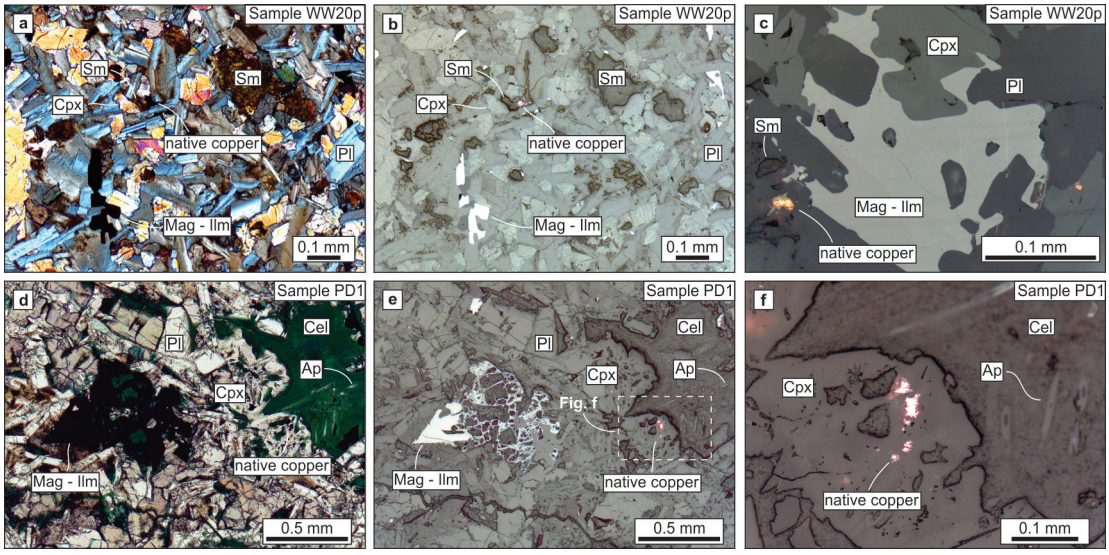

Figure 4 - Photomicrographs of paralavas with native copper. **a)** Sample WW20p showing the texture of the paralava with phenocrysts of plagioclase, clinopyroxene, magnetite-ilmenite, smectite and native copper. **b)** The same area as Figure **a** in reflected light. **c)** Detail of sample WW20p showing a phenocryst of magnetite-ilmenite and native copper in the paralava. **d)** Sample PD1 showing the texture of the paralava and areas with celadonite in plane polarized light. **e)** The same area shown in Figure **d** with reflected light highlighting the phenocrysts of magnetite-ilmenite. The dotted square shows the area with native copper. **f)** Detail of the dotted square of Figure **e** showing the relationship between crystals of clinopyroxene, native copper, celadonite and apatite in the paralava.

listed in Tables II and III. In addition, we used the chemical analyses from Ferreira (2011) in samples close to the study area. According to their chemical compositions, the host rocks are basalts, both in the diagram of Cox et al. (1979) and Middlemost (1994), available in Figure 5. The basalts are of the Paranapanema intermediate-Ti chemical type (Nakamura et al. 2003) whereas the paralavas have higher SiO_2 content similar to basaltic andesite and basaltic trachyandesite and also higher content of incompatible elements, including TiO_2. Similar relationship is observed in the samples of Ferreira (2011). On the other hand, the geochemical compositions of host basalts and paralavas are also similar to the study of D'Oriano et al. (2013), who remelted basalt tephra in the laboratory and obtained liquids enriched in incompatible elements (Figure 5). Comparatively, the analyses on samples from the Dalba quarry show that the average content of SiO_2 from the host basalt is 50.17 wt.%, similar to other basalts from the Paraná volcanic province. However, the reaction rims of paralava have increments of 2.6 wt.% in the dark reaction rim and 9.5 wt.% in the light reaction rim with contents of 51.47 wt.% and 54.96 wt.% respectively. Corresponding geochemical distribution occurs in K_2O, P_2O_5, Ba, Y, Zr, Th, U, Cu, La and other REE. All these elements are enriched in the paralavas. In the Dalba quarry, this behavior is evident and shows enrichment from the host basalts to the dark reaction rim, and even higher in the light reaction rim where plagioclase phenocrysts occur. In contrast, MgO and CaO exhibit opposite behavior. The MgO content (Figure 5) in the host basalts ranges from 6.87 wt.% to 4.93 wt.% and in the paralavas decreases to values between 4.93 wt.% and 1.38 wt.%. Analyses form Dalba quarry samples show the host basalt contents of MgO with an average approximately 4.84 wt.%. MgO gradually decreases in the paralava with 3.97 wt.% in the dark reaction rim and 2.62 wt.% in the light reaction rim. In other words, the decrease is

larger in portions where plagioclase phenocrysts are present. The same behavior is observed in CaO that has the highest concentration in the host basalts, varying between 10.97-9.05 wt.% while in the paralavas this content ranges from 7.89 to 5.5 wt.%. In samples from the Dalba quarry, the content of CaO in the host basalts showed an average of 9.5 wt.% whereas it successively decreases from the dark reaction rim (6.17 wt.%) to the light reaction rim (4.49 wt.%).

TABLE II

Chemical composition of host basalts (labeled "b") and paralavas (samples labeled "p") from the Paraná volcanic provice. Oxides in wt.%, trace elements in ppm, except Au in ppb. Below detection limit: Tl (0.1), Cd (0.3), As (5), Sb (0.2), Bi (0.1), Hg (0.1), Se (0.5), TOT/S (0.01), Cr_2O_5 (0.02). (−) = below detection limit: Ag (0.1), Cs (0.1). LOI = loss on ignition.

	Host basalts						Paralavas					
Sample	WW 18b	WW 19b	WW 20b	WW 33b	WW 34b	WW 60b	WW 18p	WW 19p	WW 20p	WW 33p	WW 34p	WW 60p
SiO_2	48.92	48.42	48.78	50.48	50.29	48.39	50.04	50.34	53.18	50.94	50.40	50.65
TiO_2	2.44	2.09	1.74	2.28	2.34	2.08	3.54	3.47	2.76	3.14	3.09	2.66
Al_2O_3	12.78	13.02	13.56	12.29	12.47	12.93	11.68	10.21	11.38	11.47	11.32	11.34
P_2O_5	0.27	0.23	0.21	0.28	0.30	0.22	0.37	0.33	0.43	0.43	0.43	0.29
Fe_2O_3	15.12	14.68	13.46	16.02	16.07	15.12	18.11	18.14	16.02	17.69	18.65	17.08
MnO	0.16	0.19	0.18	0.21	0.22	0.21	0.24	0.18	0.13	0.18	0.17	0.19
MgO	5.53	6.30	6.87	4.93	5.10	5.86	2.91	4.48	3.13	3.36	3.29	4.41
CaO	9.81	10.29	10.97	9.20	9.05	9.68	5.42	7.16	6.07	7.46	7.47	7.30
Na_2O	2.25	2.26	2.21	2.34	2.32	2.47	2.60	2.40	2.50	2.51	2.51	2.78
K_2O	1.23	0.85	0.77	1.12	1.08	1.13	3.50	1.41	2.37	1.65	1.47	2.21
LOI	1.20	1.40	1.00	0.60	0.50	1.80	1.30	1.60	1.70	0.90	0.90	0.90
TOT/C	0.03	0.03	0.02	0.05	0.02	0.09	0.02	0.03	0.03	0.02	0.02	0.04
SUM	99.74	99.76	99.78	99.77	99.76	99.92	99.72	99.72	99.68	99.74	99.71	99.82
Ag	0.1	0.1	0.1	−	−	−	0.1	0.2	0.1	0.1	0.1	0.1
Au	4.1	4.8	3.3	2.4	1.6	4.3	9.4	5.5	4.4	3.7	9.5	4.4
Ba	310	291	246	280	268	298	436	363	517	402	371	336
Be	1	1	1	1	1	1	1	2	2	2	1	1
Ce	49.1	43.6	37.8	48.5	49.2	38.6	70.9	59.2	81.4	73.1	67.4	53.9
Co	42.3	46.0	50.0	43.8	42.9	46.8	39.3	45.3	33.8	36.3	36.4	46.2
Cs	0.4	0.3	0.5	−	0.1	0.7	0.9	0.2	0.4	0.8	0.4	0.9
Cu	268	215	201	205	235	42	199	369	337	184	387	11.34
Dy	5.43	4.85	4.20	6.31	6.56	5.42	7.18	6.92	7.67	9.38	8.53	7.57
Er	3.14	2.83	2.46	4.08	4.15	3.02	4.18	3.85	4.45	5.76	5.36	3.97
Eu	1.78	1.69	1.49	1.93	1.82	1.67	2.56	2.18	2.55	2.48	2.57	2.05
Ga	20.8	20.9	20.3	20.0	20.2	21.1	22.9	21.4	22.0	21.5	20.8	21.1
Gd	5.91	5.20	4.76	7.07	6.78	5.22	7.83	7.75	8.17	9.58	9.33	6.92
Hf	4.3	3.4	3.3	4.6	4.7	3.9	6.0	5.9	7.3	7.8	6.8	5.1
Ho	1.10	0.97	0.90	1.43	1.42	1.07	1.50	1.35	1.53	1.98	1.91	1.40
La	24.2	20.6	18.4	22.8	22.7	18.6	34.4	29.0	40.1	34.6	32.9	25.3
Lu	0.38	0.38	0.35	0.57	0.55	0.41	0.57	0.52	0.61	0.78	0.77	0.55
Mo	0.6	1.1	1.0	1.2	0.8	0.6	1.2	1.1	1.1	1.2	0.8	0.7
Nb	15.3	12.9	11.1	15.2	15.2	11.8	22.7	19.2	25.6	24.0	21.3	15.8
Nd	26.8	22.9	20.8	27.6	27.0	22.3	39.4	33.4	40.1	39.7	39.9	31.1

TABLE II (continuation)

	Host basalts						Paralavas					
Sample	WW 18b	WW 19b	WW 20b	WW 33b	WW 34b	WW 60b	WW 18p	WW 19p	WW 20p	WW 33p	WW 34p	WW 60p
Ni	30.5	33.8	38.3	22.0	19.6	25.9	10.4	21.3	12.5	15.4	10.8	14.9
Pb	1.0	1.0	1.0	0.9	0.9	1.0	1.4	1.4	1.1	1.1	1.2	1.2
Pr	6.16	5.39	4.71	6.18	6.35	4.92	8.87	7.73	9.98	9.21	9.02	6.79
Rb	36.9	18.7	18.0	24.1	23.0	25.0	157.3	32.4	72.0	38.9	33.2	82.3
Sc	37	38	38	41	41	39	35	38	29	38	40	37
Sm	6.0	5.2	4.5	6.4	6.4	5.2	8.6	7.6	9.1	9.4	8.8	6.8
Sn	1	1	2	2	1	1	2	3	2	3	2	2
Sr	397	385	387	238	240	306	355	301	346	222	231	289
Ta	0.9	0.8	0.7	1.0	1.1	0.6	1.3	1.2	1.5	1.4	1.4	0.9
Tb	0.94	0.84	0.73	1.13	1.14	0.93	1.21	1.19	1.36	1.72	1.65	1.22
Th	2.5	2.7	1.9	2.4	2.0	2.5	3.5	3.6	4.7	3.9	3.7	3.4
Tm	0.42	0.42	0.36	0.61	0.58	0.46	0.59	0.55	0.62	0.76	0.75	0.63
U	0.5	0.4	0.4	0.5	0.5	0.4	0.8	0.7	0.8	0.8	0.7	0.7
V	514	504	436	458	435	450	520	800	336	424	420	599
W	0.3	0.3	0.3	0.3	0.4	0.3	0.9	0.5	0.5	0.4	0.6	0.4
Y	30.5	27.0	23.7	39.5	39.6	30.0	41.9	40.1	41.8	55.7	52.4	40.3
Yb	2.76	2.51	2.05	3.93	3.85	2.93	3.76	3.45	4.32	5.36	5.06	4.11
Zn	68	69	51	65	78	71	141	104	84	63	65	98
Zr	150	131	114	174	174	127	210	199	262	265	241	176

TABLE III

Chemical composition of host basalts (labeled "b") and paralavas (labeled "p") from Paraná volcanic province. Oxides in wt.%, trace elements in ppm, except Au in ppb. Below detection limit: Cr_2O_3 (0.02), TOT/C (0.02), TOT/S (0.01), Ag (0.3), As (5), Be (1), Bi (0.1), Hg (0.1), Sb (0.2), Se (0.5), Mo (2), W (0.5). (−) = below detection limit: Au (0.5), Cd (0.3), Ni (20), Pb (3), Sn (1), Tl (0.1). LOI = loss on ignition.

	Host basalts							Paralavas							
Sample	AS 4b	KN 22b	KN 23b	KN 24b	KN 25b	P1b	R2Pb	AS 4p	KN 22p	KN 23p	KN 24p	KN 25p	MS 36	P2p	P3p
SiO_2	51.26	49.95	50.28	50.23	49.73	49.95	50.38	51.55	52.26	50.01	51.30	54.24	56.75	54.96	51.47
TiO_2	2.10	2.11	2.15	2.13	1.81	2.2	2.26	2.09	3.03	3.51	2.84	3.05	2.06	2.26	2.66
Al_2O_3	12.97	13.33	13.32	13.37	13.32	13.07	12.65	11.93	11.21	11.39	11.99	10.36	11.23	11.03	11.30
P_2O_5	0.26	0.24	0.24	0.23	0.21	0.27	0.28	0.25	0.43	0.40	0.42	0.37	0.82	0.58	0.42
Fe_2O_3	14.75	13.87	14.10	14.19	13.95	14.30	14.58	14.85	17.01	17.67	15.92	15.40	15.18	15.31	16.11
MnO	0.21	0.21	0.20	0.20	0.19	0.21	0.17	0.18	0.21	0.22	0.17	0.34	0.17	0.16	0.17
MgO	5.04	5.62	5.67	5.91	5.98	4.73	4.95	4.93	3.28	3.78	3.38	3.61	1.38	2.62	3.97
CaO	9.23	10.04	9.95	10.06	10.18	8.87	9.26	7.89	5.59	7.31	5.78	6.99	5.05	4.49	6.17
Na_2O	2.55	2.49	2.52	2.49	2.34	2.26	2.45	2.90	2.66	2.63	2.77	2.73	2.72	2.41	2.27
K_2O	1.10	1.04	1.02	0.98	0.80	2.24	1.13	1.80	2.41	1.60	3.24	1.99	2.78	4.36	2.72
LOI	0.81	1.31	1.06	0.64	1.63	1.6	1.6	1.86	2.04	1.81	1.69	1.20	1.50	1.5	2.4
SUM	100.28	100.21	100.50	100.45	100.12	99.72	99.72	100.22	100.12	100.34	99.50	100.28	99.65	99.64	99.69
Au	5.6	5.3	4.9	6.1	6.5	2.4	-	4.3	12.5	10.8	9.0	7.7	1.7	1	7.5
Ba	320	305	338	326	265	310	298	312	556	453	488	446	727	541	433
Cd	0.37	0.94	0.57	0.65	−	-	-	−	0.49	0.66	−	0.64	−	-	-
Ce	45.2	48.4	51.6	50.1	40.3	47.6	46	45.3	94.5	81.2	85.3	74.7	128.6	85.2	68.8

TABLE III (continuation)

	Host basalts							Paralavas							
Sample	AS 4b	KN 22b	KN 23b	KN 24b	KN 25b	P1b	R2Pb	AS 4p	KN 22p	KN 23p	KN 24p	KN 25p	MS 36	P2p	P3p
Co	38.7	40.2	43.2	44.8	44.0	37.7	40	38.1	34.7	40.0	34.7	35.4	24.5	21.6	35.1
Cs	0.3	0.1	0.1	0.1	0.1	0.5	0.3	0.8	0.3	0.4	0.8	0.5	0.3	0.6	0.4
Cu	211	234	239	226	227	189	93	264	273	372	232	1315	285	600	236
Dy	6.07	5.15	5.44	5.37	5.27	4.76	5.51	6.07	8.58	7.68	8.28	6.62	12.65	9.90	7.36
Er	3.55	3.06	3.27	2.95	3.13	2.71	2.88	3.60	4.83	4.36	4.62	3.61	6.60	4.88	4.08
Eu	1.74	1.78	1.90	1.89	1.70	1.65	1.67	1.74	2.89	2.70	2.83	2.38	4.31	2.70	2.28
Ga	20.0	20.1	22.0	22.4	21.2	18.6	17.2	20.0	23.8	24.6	25.0	22	22.2	18.4	18.3
Gd	5.77	5.40	5.88	5.55	5.06	5.45	5.63	5.75	8.56	8.33	8.63	7.31	15.04	10.13	8.04
Hf	4.3	4.1	4.5	4.4	3.6	3.6	3.8	4.3	7.8	6.7	6.9	6.5	11.7	7.8	6.1
Ho	1.20	1.01	1.09	1.04	1.05	0.94	0.99	1.24	1.68	1.56	1.63	1.25	2.53	1.87	1.49
La	20.5	21.8	23.0	22.3	18.1	21.5	21.3	20.5	42.6	35.7	37.9	32.9	61.8	39.2	36.4
Lu	0.50	0.33	0.37	0.34	0.37	0.38	0.40	0.50	0.60	0.52	0.56	0.43	0.84	0.72	0.54
Nb	12.2	13.3	14.8	14.5	10.8	12.9	12.5	11.9	25.2	23.2	23.3	22.6	35.5	23.8	19.1
Nd	22.77	24.04	25.55	24.68	20.77	23.6	23.7	22.86	44.24	38.92	40.88	35.85	73.60	43.8	34
Ni	51.2	54.7	49.2	55.1	63.8	27.7	7.5	41.9	9.8	13.7	14.3	16.1	–	4.5	10.4
Pb	24.3	–	8.2	–	7.9	1.5	2.4	7.1	–	–	–	–	3.4	1.2	1.9
Pr	5.17	5.49	5.96	5.63	4.64	5.7	5.72	5.25	10.43	9.13	9.50	8.47	17.26	10.66	8.45
Rb	27.4	21.3	23.6	23.3	14.9	81.4	26.5	61.5	83.3	48.6	161.1	56.9	51.5	143.9	86.6
Sc	40	38	38	38	39	35	35	39	32	37	33	33	19	25	32
Sm	5.39	5.30	5.56	5.34	4.81	5.25	5.34	5.31	9.26	8.24	8.84	7.48	15.71	9.63	7.7
Sn	–	–	–	–	–	2	2	–	1.8	1.3	1.3	1.5	7	3	3
Sr	277	354	383	389	321	339	328	264	326	347	367	328	685	277	293
Ta	0.8	0.9	1.0	1.0	0.7	0.7	0.8	0.8	1.8	1.6	1.6	1.6	2.2	1.5	1.1
Tb	0.98	0.87	0.92	0.90	0.87	0.80	0.85	1.00	1.42	1.33	1.42	1.15	2.33	1.52	1.2
Th	2.7	2.3	2.5	2.3	2.2	2.7	2.5	2.8	4.5	3.7	3.9	3.3	6.2	5.4	4
Tl	0.11	0.14	0.14	0.11	0.12	-	-	0.19	0.21	0.41	0.34	0.33	–	-	-
Tm	0.55	0.43	0.46	0.43	0.46	0.41	0.45	0.54	0.74	0.63	0.67	0.51	0.87	0.77	0.61
U	0.5	0.4	0.4	0.4	0.5	0.6	0.7	0.5	0.9	0.7	0.8	0.5	1.3	1	0.8
V	440	433	416	442	420	476	459	492	298	497	397	556	49	230	363
Y	32.9	26.0	28.5	27.7	28.1	25.9	28	32.8	41.6	39.2	42.9	32.9	62.2	49.3	39.5
Yb	3.42	2.37	2.61	2.59	2.45	2.51	2.58	3.26	4.28	3.63	3.71	2.79	5.52	4.77	3.61
Zn	100	100	95	96	96	91	48	103	134	137	145	120	142	58	88
Zr	155	143	160	153	127	144	143	155	287	247	259	224	440	290	213

Loss on ignition of the host basalts varies between 0.5-1.8 wt.% and between 0.9-2.4 wt.% in the paralavas. In the Dalba quarry, the host basalts display an average loss on ignition of 1.6 wt.%. In the dark reaction rim, loss on ignition is 2.4 wt.% and in the light reaction rim 1.5 wt.%. This distribution shows that these rocks were affected by the H1, H2 and H3 hydrothermal events described in detail by Hartmann et al. (2012a, b, 2013).

ELECTRON MICROPROBE

The electron microprobe analyses were performed in samples of host basalts and paralavas in order to compare their mineralogy. The composition of feldspar is plotted in the ternary classification diagram Ab-An-Or (Figure 6a, b) and representative EMPA results are listed in Table IV. Overall, the feldspar of host basalts ranges in composition from

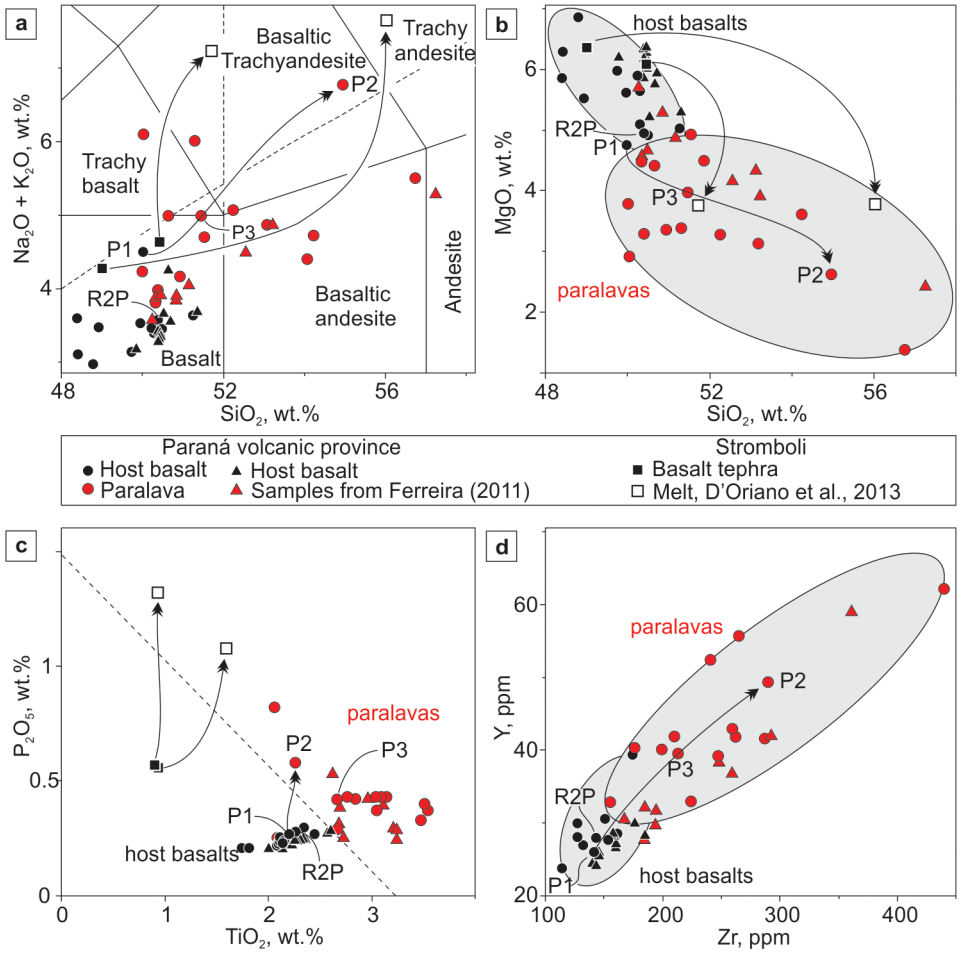

Figure 5 - Geochemical diagrams of paralavas and host basalts; arrow indicates coexisting host basalt and paralava (or melt) samples. **a)** Total alkalis-silica diagram (Middlemost, 1994) showing the composition of volcanic rocks from the Paraná volcanic province, host basalts and paralavas. Two basalt tephra compositions from Stromboli with corresponding laboratory melts (D'Oriano et al. 2013) and analyses from Ferreira (2011) were plotted for comparison. **b)** SiO_2 x MgO diagram showing the composition of the rocks of the study areas. **c)** P_2O_5 x TiO_2 diagram showing the two fields of host basalts and paralavas. **d)** Zr x Y diagram highlighting the enrichment in both elements between the host basalts and the paralavas.

An_{50} to An_{70} (labradorite), but several analyses are more sodic. On the other hand, the plagioclase in the paralavas presents compositions between An_{30} and An_{50} (andesine) and some analyses are labradorite, a more sodic composition than in the host basalts. The alkali feldspar of host basalt and paralavas is essentially composed by sanidine. Most analyses of KF in the host basalt are sanidine compositions between Or_{55-80}. Some analyses are Or_{99} and some individual analyses plot in the orthoclase field. In the paralavas, the sanidine displays Or_{35-85} and a few analyses plot in the orthoclase field.

Clinopyroxene was observed in both host basalt and paralava. According to the classification of Morimoto et al. (1988), augite and pigeonite are present in the host basalt, and only augite in the paralavas (Figure 6c, d; Table V). In the host basalt, the clinopyroxene is present in the matrix and also as sparse microphenocrysts; in the paralavas, clinopyroxene occurs only as phenocrysts. The

variation of pigeonite composition in the host basalt is Wo_{7-20} (Figure 6d). The augite composition in the host basalt ranges from Wo_{26-41} with slightly higher Mg content than that observed in the augite from paralavas. On the other hand, the augite composition in the paralavas displays compositions between Wo_{27-42} and has in general higher iron content than augite from the host basalt.

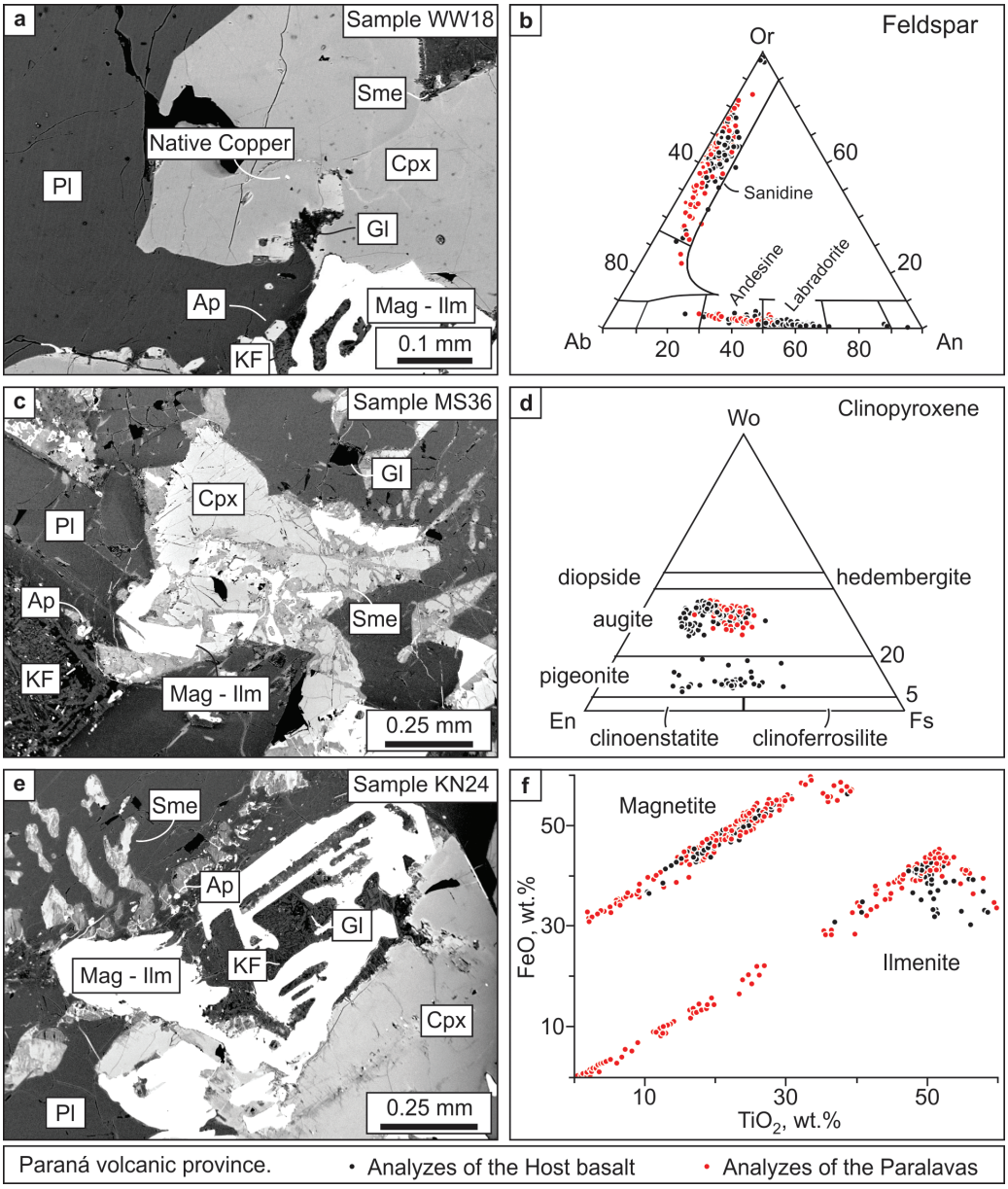

Figure 6 - Back-scattered electron images and classification diagrams of feldspar, clinopyroxene and magnetite-ilmenite. **a)** Back-scattered electron image highlighting the phenocrysts of plagioclase and the interstitial presence of KF and glass. **b)** Ternary Ab-An-Or diagram of feldspar. **c)** Back-scattered electron image highlighting the phenocrysts of clinopyroxene. **d)** Ternary En-Wo-Fs diagram of clinopyroxene. **e)** Back-scattered electron image highlighting the phenocrysts of magnetite – ilmenite. **f)** Binary diagram FeO x TiO_2 showing the fields of magnetite and ilmenite of paralavas. Symbology: black dot = host basalt, red dot = paralava, Pl = plagioclase, Cpx = clinopyroxene, KF = potassium feldspar, Mag-Ilm = magnetite-ilmenite, Ap = apatite, Sme = smectite, Gl = glass.

TABLE IV
Representative electron microprobe analyses of feldspar from host basalts and paralavas (wt.%).

	Host basalts								Paralavas							
	Alkali Feldspar				Plagioclase				Alkali Feldspar				Plagioclase			
Sample	KN24b	PD1	WW18b	WW20b	KN22b	KN24b	PD1	WW20b	KN22p	KN24p	MS36	PD1	KN24p	MS36	PD1	WW20p
SiO_2	73.44	65.10	66.47	61.57	52.52	54.26	56.88	52.40	75.94	72.52	66.0	69.54	55.09	55.85	57.94	55.91
TiO_2	0.19	0.86	0.00	1.78	0.09	0.10	0.07	0.10	0.29	0.14	0.09	0.09	0.10	0.10	0.05	0.09
Al_2O_3	11.15	15.98	17.67	15.19	28.95	27.77	27.05	29.09	10.39	13.47	18.17	16.53	26.53	27.13	26.14	27.00
Cr_2O_3	0.00	0.00	0.00	0.00	0.00	0.00	0.00	0.00	0.00	0.00	0.00	0.00	0.00	0.00	0.00	0.00
Fe_2O_3	3.82	1.02	0.06	8.09	0.99	1.10	0.85	1.14	2.98	0.17	0.38	1.10	0.72	0.57	0.58	0.63
Mn_2O_3	0.04	0.05	0.00	0.00	0.00	0.00	0.02	0.04	0.00	0.00	0.00	0.03	0.03	0.00	0.00	0.01
MgO	1.27	0.92	0.01	3.05	0.09	0.07	0.02	0.09	0.85	0.00	0.00	0.65	0.07	0.09	0.05	0.11
CaO	0.54	0.27	0.00	0.67	12.33	11.16	9.27	12.51	0.33	0.56	0.04	1.13	10.24	9.91	8.53	9.93
Na_2O	1.83	2.65	0.05	2.27	4.52	5.07	6.03	4.36	2.01	4.23	2.24	5.25	5.45	5.87	6.18	5.65
K_2O	7.35	10.73	16.20	9.17	0.31	0.45	0.50	0.27	6.33	5.81	13.08	5.35	0.51	0.50	0.61	0.48
BaO	0.06	0.07	0.00	0.08	0.00	0.01	0.05	0.00	0.06	0.44	0.08	0.08	0.00	0.01	0.05	0.01
Total	99.69	97.64	100.47	101.86	99.81	99.98	100.75	100.01	99.19	97.35	100.07	99.75	98.74	100.04	100.12	99.83
Si	3.26	3.03	3.04	2.81	2.40	2.46	2.54	2.39	3.34	3.26	3.01	3.08	2.52	2.52	2.60	2.53
Al	0.58	0.88	0.95	0.82	1.56	1.49	1.43	1.56	0.54	0.71	0.98	0.86	1.43	1.44	1.38	1.44
Fe_3	0.13	0.04	0.00	0.28	0.03	0.04	0.03	0.04	0.10	0.01	0.01	0.04	0.02	0.02	0.02	0.02
Mn_3	0.00	0.00	0.00	0.00	0.00	0.00	0.00	0.00	0.00	0.00	0.00	0.00	0.00	0.00	0.00	0.00
Cr	0.00	0.00	0.00	0.00	0.00	0.00	0.00	0.00	0.00	0.00	0.00	0.00	0.00	0.00	0.00	0.00
Ti	0.01	0.03	0.00	0.06	0.00	0.00	0.00	0.00	0.01	0.00	0.00	0.00	0.00	0.00	0.00	0.00
su1	4.06	4.03	4.00	4.18	3.99	3.99	4.00	4.00	4.05	3.99	4.01	4.03	3.99	3.99	4.00	4.00
Ba	0.00	0.00	0.00	0.00	0.00	0.00	0.00	0.00	0.00	0.01	0.00	0.00	0.00	0.00	0.00	0.00
Ca	0.03	0.01	0.00	0.03	0.60	0.54	0.44	0.61	0.02	0.03	0.00	0.05	0.50	0.48	0.41	0.48
Na	0.16	0.24	0.00	0.20	0.40	0.45	0.52	0.39	0.17	0.37	0.20	0.45	0.48	0.51	0.54	0.50
K	0.42	0.64	0.95	0.53	0.02	0.03	0.03	0.02	0.36	0.33	0.76	0.30	0.03	0.03	0.03	0.03
su2	0.60	0.89	0.95	0.77	1.02	1.02	1.00	1.01	0.54	0.74	0.96	0.81	1.02	1.02	0.98	1.00
Components																
An	0.04	0.02	0.00	0.04	0.59	0.53	0.45	0.60	0.03	0.05	0.00	0.07	0.49	0.47	0.42	0.48
Ab	0.26	0.27	0.00	0.26	0.39	0.44	0.52	0.38	0.32	0.50	0.21	0.56	0.48	0.50	0.55	0.49
Or	0.69	0.72	1.00	0.69	0.02	0.03	0.03	0.02	0.65	0.45	0.79	0.37	0.03	0.03	0.04	0.03

TABLE V

Representative microprobe analyses of clinopyroxenes from host basalts and paralavas (oxides in wt.%).

	Host basalt								Paralavas							
	Augite				Pigeonite				Augite							
Samples	KN22b	KN24b	PD1	WW18b	KN22b	KN24b	WW18b	WW20b	KN22p	KN24p	KN24p	MS36	MS36	PD1	PD1	WW20p
SiO_2	50.87	50.19	51.02	50.42	50.80	50.32	51.25	50.78	50.15	50.23	49.68	49.88	49.59	50.57	50.05	50.25
TiO_2	0.92	0.86	1.23	0.79	0.43	0.48	0.46	0.46	0.98	0.81	0.95	0.72	1.11	0.96	1.06	1.01
Al_2O_3	1.36	1.47	1.40	1.06	0.53	0.77	0.62	0.62	1.55	1.35	1.79	0.95	2.13	1.55	1.65	1.69
Cr_2O_3	0.02	0.00	0,01	0.02	0.01	0.01	0.00	0.00	0.05	0.00	0.01	0.00	0.00	0.05	0.00	0.01
FeO	15.04	15.63	16.25	18.24	27.17	26.68	26.26	25.25	17.21	15.02	15.09	19.94	17.41	15.47	16.58	15.71
MnO	0.41	0.35	0.36	0.41	0.56	0.58	0.58	0.51	0.39	0.35	0.28	0.49	0.46	0.28	0.40	0.31
MgO	13.85	13.94	13.77	12.08	15.34	15.50	17.06	16.97	12.73	13.81	13.59	10.64	10.89	12.79	13.29	13.33
CaO	16.88	17.32	16.16	16.97	4.78	4.56	4.53	4.30	16.44	16.99	17.31	16.53	17.32	17.63	16.48	16.85
Na_2O	0.22	0.29	0.23	0.23	0.06	0.05	0.06	0.06	0.22	0.25	0.25	0.25	0.31	0.26	0.20	0.22
K_2O	0.03	0.03	0.00	0.01	0.00	0.05	0.00	0.01	0.00	0.03	0.01	0.01	0.11	0.03	0.00	0.00
Total	99.60	100.09	100.45	100.23	99.68	99.00	100.82	98.96	99.72	98.85	98.96	99.39	99.33	99.60	99.71	98.38
Atoms per formula unit calculated on the basis of 6 oxygen																
Si	2.25	2.22	2.24	2.24	2.27	2.26	2,25	2.27	1.93	1.93	1.91	1.95	1.92	1.94	1.92	1.93
Ti	0.03	0.03	0.04	0.03	0.01	0.02	0.02	0.02	0.03	0.02	0.03	0.02	0.03	0.03	0.03	0.03
Al	0.07	0.08	0.07	0.06	0.03	0.04	0.03	0.03	0.07	0.06	0.08	0.04	0.10	0.07	0.07	0.08
Cr	0.00	0.00	0.00	0.00	0.00	0.00	0.00	0.00	0.00	0.00	0.00	0.00	0.00	0.00	0.00	0.00
Fe	0.56	0.58	0.60	0.68	1.02	1.00	0.96	0.94	0.55	0.48	0.49	0.65	0.56	0.50	0.53	0.50
Mn	0.02	0.01	0.01	0.02	0.02	0.02	0.02	0.02	0.01	0.01	0.01	0.02	0.02	0.01	0.01	0.01
Mg	0.91	0.99	0.90	0.80	1.02	1.04	1.12	1.13	0.73	0.79	0.78	0.62	0.63	0.73	0.76	0.76
Ca	0.80	0.82	0.76	0.81	0.23	0.22	0.21	0.21	0.68	0.70	0.71	0.69	0.72	0.72	0.68	0.69
Na	0.02	0.02	0.02	0.02	0.01	0.00	0.02	0.01	0.02	0.02	0.02	0.02	0.02	0.02	0.01	0.02
K	0.00	0.00	0.00	0.00	0.00	0.00	0.00	0.00	0.00	0.00	0.00	0.00	0.01	0.00	0.00	0.00

The opaque minerals are approximately 0.1 to 0.2 mm in size in the matrix and also occur as anhedral phenocrysts with skeletal habit and showing some alteration. The electron microprobe analyses of magnetite and ilmenite are plotted in the binary diagram FeO *versus* TiO_2 (Figure 6e, f) that shows positive correlation between the two minerals. Representative EMPA results are listed in Table VI. The magnetite-ilmenite pair has similar compositional distribution in both the host basalts and the paralavas. However, the magnetite from paralavas has slightly higher FeO and TiO_2 content than the host basalt. The analyses of ilmenite from paralavas show a wide distribution of FeO and TiO_2 contents but in the high FeO and high TiO_2 analyses, the ilmenite of paralavas has higher FeO and similar TiO_2 content than the host basalts. The occurrence of magnetite and ilmenite is linked to the presence of native copper in paralavas (Figure 7) similar to the relationship of copper mineralization with clinopyroxenes, smectite and celadonite.

FLUID INCLUSIONS

Four double polished thin sections of sample PD1 (P1C, P5, P6 and P7) were prepared for analyses of fluid inclusions. The most common size of fluid inclusions is 5-10 μm. In P1C, 8 (eight) fluid inclusions were evaluated, although the data were obtained in only 4 fluid inclusions due to their tiny dimensions. In these inclusions, salinities range from 5.6 to 7.3 wt.% eq. NaCl, but the results were disregarded because many of these inclusions have suggestive behavior of metastability. In thin section P5 57 fluid inclusions were investigated. Although the majority has small dimensions between 5 and 10 μm some reach 12 μm, 17 μm and 25 μm. Some have suggestive features of melt inclusions (Figure 8a), while the largest fluid inclusions have leakage features and necking down and were not measured. Part of the fluid inclusions is composed of aqueous saline solutions, although some of them are metastable. The Tfg (ice melting temperature)

TABLE VI
Representative microprobe analyses of magnetite and ilmenite from host basalts and paralavas (oxides in wt.%).

	Host basalt							Paralavas						
	Magnetite				Ilmenite			Magnetite				Ilmenite		
Sample	KN22b	PD1	WW20b	WW20b	KN22b	PD1	WW18b	WW20b	KN22p	KN24p	MS36	PD1	KN22p	MS36	PD1	WW20p
TiO_2	20.70	24.63	14.68	18.47	49.56	50.04	49.54	49.79	20.35	23.64	29.70	27.65	51.19	48.20	50.64	50.89
Al_2O_3	1.58	1.40	1.87	2.68	0.00	0.00	0.00	0.00	1.23	1.33	0.31	0.68	0.00	0.08	0.00	0.00
Cr_2O_3	0.20	0.15	0.45	0.24	0.00	0.03	0.05	0.01	0.03	0.23	0.05	0.03	0.00	0.01	0.01	0.01
Fe_2O_3	24.32	16.09	36.16	26.76	5.22	4.51	6.64	5.53	26.78	20.01	6.96	11.22	3.49	2.66	3.72	1.03
FeO	48.11	49.93	42.98	45.16	42.43	38.60	41.20	40.85	48.57	50.69	55.52	54.10	44.33	41.53	44.05	44.38
MnO	0.43	2.35	0.17	1.79	0.42	5.19	0.40	0.43	0.44	0.72	0.75	0.64	0.63	0.45	0.93	0.65
MgO	0.48	0.16	0.60	0.16	0.97	0.65	1.66	1.96	0.30	0.65	0.29	0.31	0.60	0.77	0.31	0.41
Total	95.81	94.72	96.91	95.26	98.59	99.02	99.49	98.58	97.70	97.28	93.59	94.63	100.25	93.70	99.66	97.36

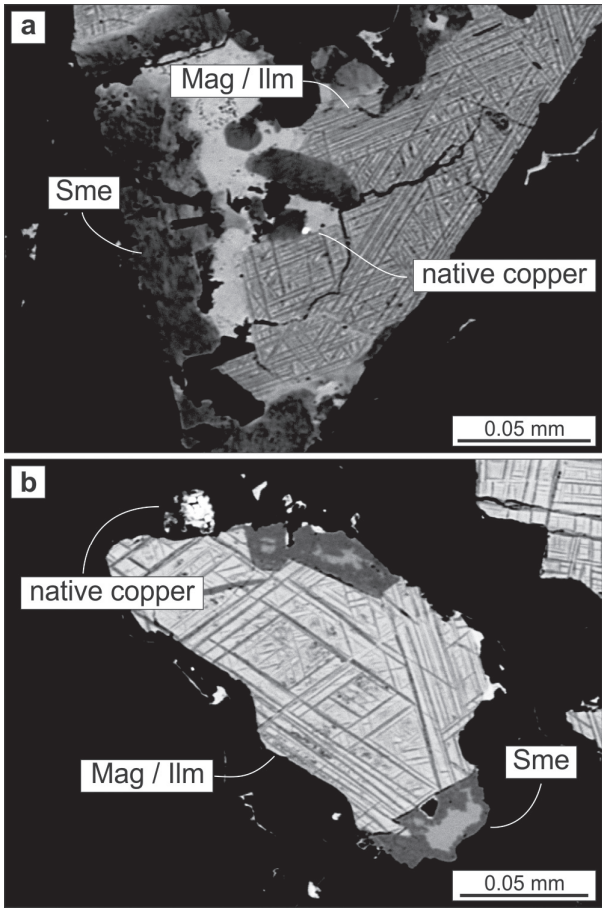

Figure 7 - Back-scattered electron images. **a, b)** Relationship between magnetite-ilmenite, smectite and native copper in the paralava. Symbology: Mag-Ilm = magnetite-ilmenite, Sme = smectite.

in negative temperature was repeated in several runs. In these cases, the salinity ranged from 13.9 to 16.1 wt.% eq. NaCl. Some of the fluid inclusions are dark and distorted, but repeated cooling to -180 °C showed no change in phase. This seems to indicate the presence of CO_2 or mixtures of CO_2 with other volatiles, unless the inclusions have extremely low densities such as water vapor, CO_2 gas or CH_4 gas. Phase changes were not observed with microthermometry. In thin section P6, 43 fluid inclusions were analyzed. The fluid inclusions are rounded and a few are black, elongated or distorted (Figure 8b). The main size of fluid inclusions is from 5-15 μm, but some are 20 to 40 μm. The microthermometric measurements in these fluid inclusions presents dubious results. The system H_2O + NaCl + $CaCl_2$ (+/- $MgCl_2$) is cautiously suggested with salinity ranging approximately from 14 to 16 wt.% eq. NaCl. A clear single-phase inclusion cooled down to -180 °C and presented no changes, showing that it may consist of a solid or of a low-density fluid undetectable by microthermometry (CO_2 gas, CH_4 gas or water vapor). There is also a secondary fluid inclusion (~100 μm), entrapped at low temperature with suggestive leakage features, and displaying very different low salinity (2.30 wt.% eq. NaCl), morphology, behavior and size from other fluid inclusions observed.

In thin section P7, 18 fluid inclusions were analyzed. The sizes vary from 5 to 10 μm and only one is 17 μm with suggestive features of melt. The bubbles within the fluid inclusions are small. During the heating of these fluid inclusions, the temperature was raised to 600 °C with no change in any of the inclusions analyzed. In all thin sections, the eutectic temperatures of the aqueous phase ranged mainly from – 60 °C to – 50 °C, suggestive of an aqueous system comprising NaCl + H_2O + $CaCl_2$ (+/- $MgCl_2$). Nevertheless, these results are often dubious due to the small size of the inclusions and the occurrence of metastability.

DISCUSSION

The field observation of the formation of paralavas as reaction rims within the host basalt precludes any interpretation of the paralavas as products of fractional crystallization. Although the products of remelting of the host basalt may be chemically similar to fractional crystallization, the process is overall comparable to the remelting of volcanic blocks entrained in lava (D´Oriano et al. 2013). All previous investigations considered fractional crystallization as the main process responsible for the enrichment of the lava in incompatible elements and its ascent to the upper part of the lava core (Table VII). But some geochemical

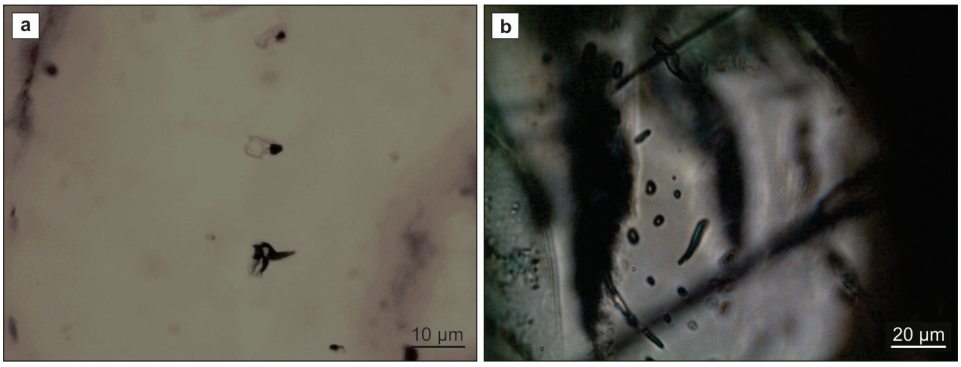

Figure 8 - Fluid inclusions in plagioclase crystals (sample PD1). **a)** Thin section P51B with features of melt inclusions. Highlight for the small size of the melt inclusions. **b)** Thin section P6 with darkened fluid inclusions. The morphology ranging from regular (rounded) to elongated, with variable dimensions. These inclusions may be composed of a low-density fluid (water vapor, CO_2 or CH_4).

features cannot be explained entirely with use of fractional crystallization. For instance, the study of Greenough and Dostal (1992a) showed that the presence of the rhyolite layers and pegmatite in the North Mountain basalt flows cannot be explained by fractional crystallization. Mass balance calculations of the major elements have missing phases, which in that study is represented by stilpnomelane. The authors suggested that the rhyolite layers and the pegmatite are product of silicate liquid immiscibility. The study of Hartley and Thordarson (2009) concluded that although "...crystal fractionation exerts a first-order control on the Grande Ronde basalt composition, it is generally agreed that fractional crystallization alone is not sufficient to explain the compositional and isotopic variations observed in the Grande Ronde basalt. Both mantle heterogeneity and crustal contaminations are advocated as possible explanations for these variations."

The abundant glass observed in the groundmass of all pegmatite lenses and the presence of large (10 cm), curved, hollow crystals requires quenching of the lava. This texture is observed in all pegmatite lenses described in continental basalts in other provinces and in the Paraná volcanic province.

TABLE VII
Two main hypotheses on the origin of paralavas (previously known as basaltic pegmatites or segregation sheets).

Origin	Main observation	References
Methane streaming forms paralava, buoyant rise	Pyrometamorphism of kerogen-rich shales at depth (Irati Formation) by intruding basalt magmas liberates CH_4. Streaming of methane through crystalline basalt at 1,000 ºC causes melting (75%) of host basalt and buoyant rise of paralava, resulting in later quench-crystallization of clinopyroxene and other minerals in a glassy matrix.	This work
Fractional crystallization, buoyant rise	In the Levering lava of the Columbia River province, "…the segregated melt is generated by fractional crystallisation from a crystal mush horizon within the basal zone of the lava flow, and rises buoyantly through the flow." "Extraction of enriched intercrystalline material." Magma structure rigid but plastic, forming lenses of residual liquid.	Hartley and Thordarson 2009. Other references, similar origin: Cornwall 1951, Puffer and Horter 1993, Marsh 1995, Philpotts et al. (1996 and 1999), Dragovic and Philpotts 2002, Philpotts and Dickson 2002, Cheadle et al. 2004, Greenough and Dostal 1992b, Greenough et al. 2004, Ferreira et al. 2014.

For instance, in Hawaii, segregation veins occur in entirely crystalline diabase and contain ~30 vol.% glass matrix (Fodor and Bauer 2014). The geochemistry of these veins and host basalts is similar to the Paraná volcanic province occurrences. The reason for the presence of undevitrified glass in these pyrometamorphic rocks remains largely unexplained in general (Grapes 2011).

There is no reasonable explanation for the presence of higher temperature liquid lava in the lower core of a thick, solid lava flow, or for its quenching against comparable-temperature host rock. There is also no known fractional crystallization process that would raise the temperature of cooling basalt above its liquidus temperature to cause remelting of the lower core. An extraneous source of energy seems required to cause remelting of the crystalline basalt. We suggest the combustion of methane as the cause of remelting of basalt and formation of the paralava. It is therefore necessary to examine the steps involved in the process, including the source of the methane, its non-reactive ascent in the crust, spontaneous combustion in the lower core of the lava, the temperature attained during combustion, remelting of the crystalline basalt (paralava formation), and injection of the paralava upwards into the core and quenching of the paralava.

The methane present in sedimentary basins in general may have originated from mantle degassing, anaerobic bacterial reduction of organic matter or thermal cracking of kerogen. The Paraná Basin contains several sedimentary formations rich in kerogen under the Paraná volcanic province. The two most significant ones are the coal-rich, Permian Rio Bonito Formation present in 10% of the basin in its southeastern portion, and the Devonian Ponta Grossa Formation and Permian Irati Formation present along the entire basin. Bituminous shales are also present in the Serra Alta Formation higher up in the stratigraphy.

The injection of basaltic sills into coal seams turns kerogen mostly into CO_2. "Humic coals are mainly composed of Type III kerogen from which 10–25% of the carbon mass can be converted into gas" whereas "…type I and II kerogen commonly found in organic-rich shales have the potential of converting up to 95% of the TOC to hydrocarbons…" (Aarnes et al. 2010). Because the coal seams cover a minor area of the Paraná Basin and coal generates mostly CO_2, the bituminous shales of the Irati Formation are more significant for our modelling. In several continental volcanic provinces, "in shales with total organic carbon content (TOC) >5 wt.%, CH_4 is the dominant volatile ... generated through organic cracking, relative to H_2O generation from dehydration reactions ..." (Aarnes et al. 2010). Type I and II kerogen is commonly found in organic-rich shales such as the Irati Formation and may convert up to 95% of the TOC to hydrocarbon. Low oxygen fugacity in organic-rich shales will originate fluid dominated by CH_4–H_2O rather than H_2O–CO_2 in contact aureoles (Aarnes et al. 2010). It can be assumed therefore that kerogen will convert mostly into CH_4 rather than CO_2 in contact metamorphism of shale. CH_4 will dominate for TOC contents of >5 wt.%, while H_2O will dominate for TOC contents of <1 wt.%. In the Paraná Basin, particularly in the state of Paraná, TOC contents of the bituminous shales of the Assistência Member (Irati Formation) have TOC contents between 10-25% (Pereira 2013).

Basaltic sills are present under the Paraná volcanic province in a large volume. Mariani et al. (2013) concluded from gravimetric modeling that sills up to 10,000 m in integrated thickness are present in the crust below the 1,500 m thick lavas. Extensive drilling (n = 1424 holes) for coal-seam evaluation by the Geological Survey of Brazil in 1986 resulted in a clear picture of the number and thickness of sills (Table VIII) injected into the sedimentary basin (southeastern coal-bearing portion). The examination of 835 logs that include the Irati Formation and the Rio Bonito Formation shows that basaltic sills are present dominantly in

TABLE VIII
Number of drill cores containing sills and average thickness of basaltic sills in sedimentary formations from the southeastern portion of the Paraná Basin; based on compilation of 835 cores drilled in the coal basin by CPRM in 1986.

Formation	Number	Average thickness, m
Serra Alta	42	22
Irati	377	23
Palermo	31	12
Rio Bonito	109	18
Itararé	13	27

the Irati Formation, followed by the Rio Bonito Formation and the other formations. The field observation in quarries confirms the dominance of sills in the Irati Formation over the other formations. The fissile nature of the Irati Formation shales seems to have facilitated the injection of the magmas (e.g., Araújo et al. 2004) compared to the dominantly fine-grained sandstones of the other formations. The average thickness of the sills is near 20 m for all formations. The Irati Formation thus emerges as one target for the observation of pyrometamorphism of bituminous shales in the Paraná Basin.

The sedimentary rocks of the Paraná Basin contain therefore the necessary large volume of kerogen, spread over the entire basin, as potential generator of methane; part of the kerogen was cracked and a large volume still remains in the sedimentary basin. The large number of basaltic sills injected into the bituminous beds offers additionally the necessary heat for the secondary cracking of kerogen into methane. The newly-formed gas is modelled to migrate upwards unreactive through the sedimentary and the consolidated (cool) volcanic pile. The temperature of the sedimentary rocks, and contained (and ascending) fluids including methane, is estimated at 60 °C above the temperature expected for intraplate basins. This additional heat probably originated in volcanism, mostly from sills. Evidence in this sense is found in the microthermometric studies of primary fluid inclusions in calcite from fractures (Cesário Lange region, São Paulo state) indicating that aqueous fluids were trapped at "70-141 °C, with the highest mode at 105 °C; salinity is between 5.33-0.0 wt.% eq. NaCl" (Sawakuchi et al. 2011). The highest temperature attained is constrained by mineral assemblies and oxygen isotopes at <200 °C. At this temperature, methane is not ignited and flows through the sedimentary layers toward the top; a much higher temperature is required to ignite methane. The autoignition temperature of methane is 580 °C in air, which is the minimum temperature required to ignite the gas in air without a spark or flame being present (Wikipedia). As mentioned by Caron et al. (1999), "the autoignition temperature ... is strongly pressure-dependent and decreases with increasing pressures", but is not expected to decrease down to the temperature present in the Paraná Basin sedimentary rocks below the Paraná volcanic province. In our model, methane gas was capable to migrate upwards through the sedimentary package without spontaneous reaction with oxygen present in pores and in mineral lattices.

As the gas reached the base of the uppermost flow that was still cooling at a temperature around 1000 ° C (without having yet developed columnar jointing) the scenario became entirely different. A coincidence of timing occurred between the processes of methane generation in the Irati Formation and its arrival at the base of the uppermost cooling basalt. According to Aarnes et al. (2010), "the generation of volatiles is occurring on a time-scale of 10–1000 years within an aureole of a single sill…" This is the same time-scale of cooling of a basalt lava. In the studies of a 45 m thick basaltic andesite flow from the Paraná volcanic province, Schenato et al. (2003) estimated the time for complete solidification as 35 years, corresponding to cooling processes between the liquidus (1200 °C) and the solidus (1000 °C) of the lava. During cooling, the two solidus curves approaching from above and below intersected at two-thirds distance

from the top of the flow; the temperature reached 1000 °C and the flow became solid. This level coincides with the position commonly attributed by many authors for the origin of the segregation melts. Cooling of the 45 m thick lava to ambient temperature probably lasted 560 years (Schenatto et al. 2003).

Only very few thin basalt lavas have pegmatite seams, and these are of the order of millimeters in thickness; we interpret this as due to the faster cooling of the lava. Methane did not ignite as it passed through this thin flow. Thicker (>70 m) lavas and mafic plutonic complexes remain at a high temperature for a longer period of time. Because the vertical cooling joints of thick lava flows begin to form at 1,000-900 °C and do not contain injected paralavas, these must have formed at a temperature >900 °C. In one study, the initiation of surface cracks in a cooling lava lake from Hawaii was observed to occur at 900 °C for a lava emplacement temperature of 1090 °C (Peck and Minakami 1968).

Methane is extremely flammable and is violently reactive with oxidizers (e.g., Wikipedia). In the cooling basalt, little free oxygen (the prime example of oxidizer agent) is present so methane reacts with the oxygen in the mineral lattices in a reaction of "reduced burning". This is a strongly exothermic chemical reaction. The local temperature in the holocrystalline, cooling (1,000 °C) basalt is raised because of CH_4 oxidation. Several geological estimates have been made on the temperature attained during methane burning. For instance, Grapes (2011) estimates the temperature in air up to 1,600 °C, whereas Sokol et al. (2010) refer to ultrahigh temperature up to 1,500 °C in ignition foci of sedimentary rocks by combustion metamorphism. A detailed study of mud melting by methane ignition established the temperature at 1,400-1,800 °C, with the resultant formation of glass at 1,400 °C and lower.

We thus model the remelting of the base of the basalt lava core as a consequence of temperature rise from the natural cooling lava at 1,000 °C up to 1,600 °C. At this very high temperature, the affected basalt would melt extensively, possibly 75% liquid with 25% remaining solid. This is the inverse proportion commonly mentioned for the extent of fractional crystallization required to generate the pegmatite sheets in other provinces. The description of segregation sheets by Philpotts et al. (1996), for example, concludes from fractional crystallization modelling that "the composition of the segregations corresponds to liquids that can form by as little as 25% crystallization of the initial basalt." The resultant new magma may be overall similar by the two processes. The mixed rock that remains in place would be composed of a large portion of crystallized new magma and a small portion of remnant, unfused solid. In the terminology of Grapes (2011), this may be called a buchite, which is a partially fused rock by pyrometamorphism.

In a relevant study for the present interpretation, D'Oriano et al. (2013) remelted Etna, Vesuvius and Stromboli basalt tephra in the laboratory and obtained liquids enriched in incompatible elements and SiO_2 and impoverished in Mg. In the present study, similar results were observed in EMPA analyses of magnetite, which displays higher contents of TiO_2 in the paralavas than in the host basalt. The chemical composition of samples P1 (host basalt), P2 and P3 (reaction rims of paralavas) have similar behavior, including Zr and Y. This observation supports the comparison between remelting in paralavas of Paraná volcanic province with those obtained in the laboratory.

The overall process is shown in the model (Figure 9) that explains the origin of the newly-formed liquid in the lower portion of the lava core. The paralava contains a higher proportion of light elements, so it is more "differentiated" and rises buoyantly through stockworks to the central and upper portions of the core. Dikes and sills of paralava are thus formed in the core of thick basaltic flows. The columnar jointing will be formed later

by cooling of the flow below 900 °C, with the paralava already solid with intersertal texture and part of the coarse-grained host basaltic rock.

We envisage the occurrence of similar processes of basalt or gabbro remelting to form paralavas in other continental provinces whenever methane streaming occurred through solid rock portions at 1000 °C and methane autoignition occurred. The recognition of the process is most significant for petrology and economic geology. The presence of CH_4 in fluid inclusions (Larsen et al. 1992) was attributed to carbon assimilation from sedimentary blocks. In the fluid inclusions evaluated in the paralavas from the Paraná volcanic province, the $NaCl+H_2O+CaCl_2$ system was suggested as a hypothesis. This system can be observed in a wide range of geological environments and also in the sedimentary basins with hydrocarbon occurrences (Steele-MacInnis et al. 2011) such as the Paraná Basin. Overall, the evaluation of this study indicates at least two distinct phases of trapped fluid inclusions. The older generation was trapped at higher temperatures from a higher salinity fluid, which may contain a volatile of low-density, besides single-phase inclusions consisting only of this volatile species. Fluid inclusions of later generation were entrapped under low temperature conditions from low salinity solutions which may be related to the Cretaceous hydrothermal events described by Hartmann et al. (2012a) and superimposed on these rocks. On the other hand, the presence of CH_4 in the fluid inclusions in the

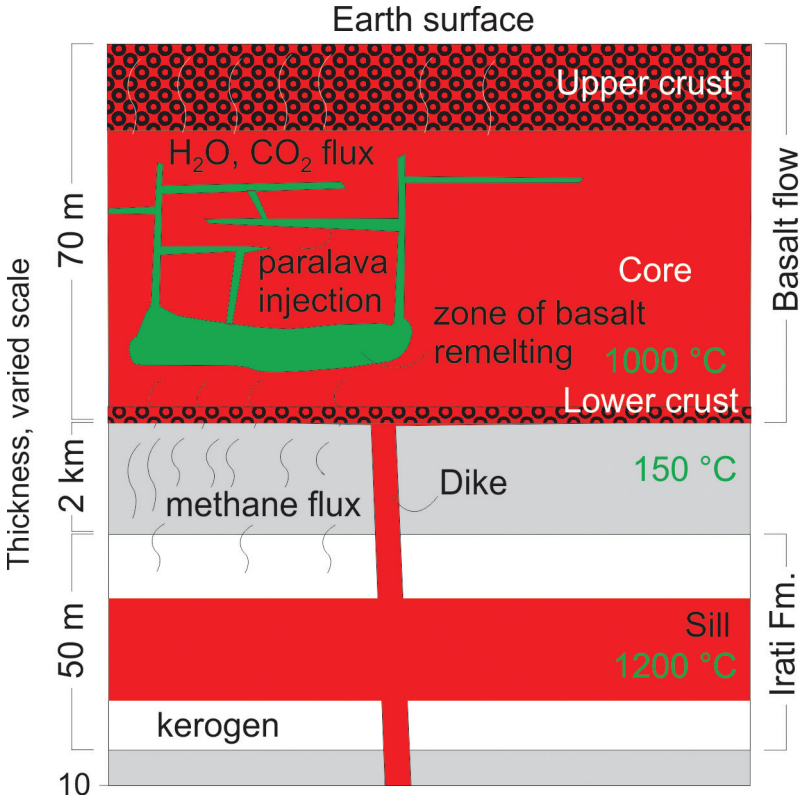

Figure 9 - Paralava genetic model, starting with the cracking of kerogen from the Irati Formation to form methane. Upward flow of methane through sedimentary formations and volcanic pile of the Paraná Basin. Autoignition of methane in the lower portion of a thick cooling flow (1,000 °C), elevating temperature to approximately 1,500 °C. Host basalt melt and paralava sill and dike injection in the core of the flow.

paralavas of Paraná volcanic province has not been definitively identified because of the small size of inclusions. However, the cooling results indicate that the fluid inclusions may be constituted by a low density fluid such as water vapor, CO_2 or CH_4 undetectable by microthermometry. Further Raman studies of fluid inclusions with appropriate size may confirm the presence of CH_4.

The economic importance of paralavas opens a new frontier for studies related to mineral exploration. This can be illustrated with the copper mineralization in the paralava of Dalba quarry, in which the copper average in the host basalts is 141 ppm (n = 2), slightly below the average (152 ppm) established for the volcanic province (Crocket 2002). On the other hand, in the dark reaction rim, the copper content increases to 236 ppm, reaching 600 ppm in the light reaction rim. This shows that the concentration of metal was related with the paralava generation process. The host basalt presents LOI = 1.6 wt.%, similar to the LOI of the light reaction rim (1.5 wt.%), while the LOI of the dark reaction rim is 2.4 wt.%. The native copper mineralization in the host basalt is associated to the dendrites at the surface of columnar joints and is consistent with the epigenetic hydrothermal mineralization generated during the H1, H2 and H3 Cretaceous hydrothermal events (for details see Hartmann et al. 2012a, b) which promoted hydrothermal alteration of the host basalts and paralavas. The native copper occurrences observed in the paralavas filled microcavities in the light reaction rim and the higher Cu contents are associated with paralavas bodies.

The geological and mineralogical evidence thus far described in pegmatites and some segregation sheets in thick basalt lavas and in intrusions were previously attributed to fractional crystallization, but may be alternatively explained by partial melting process, including the Paraná basaltic province and possibly other similar flood basalt and mafic intrusions in the world. We thus use "paralava" for these geological bodies, as an interpretation of the remelting of the host basalt by the heat generated from combustion of methane confined within a thick, cooling basalt flow or intrusion.

CONCLUSIONS

Rocks from the Paraná volcanic province previously designated pegmatites or segregation sheets are presently interpreted as paralavas, the result of melting of hot host basalts by methane combustion. The paralavas generated by remelting (1,600 ºC) of the lower portion of the still-hot (1,000 ºC) core of the host basalt and rose buoyantly to inject the core of the flow. The external source of energy required to raise the temperature was the reaction of methane with the hot minerals (silicate and oxides). The methane was originated deeper in the Paraná Basin from the cracking of kerogen in bituminous shales (Ponta Grossa, Irati Formation and others).

ACKNOWLEDGMENTS

Financial support was provided by Project from Conselho Nacional de Desenvolvimento Científico e Tecnológico (CNPq)/VALE, Ministério da Ciência e Tecnologia (MCT) and Fundo SETOR Mineral (CT-Mineral) entitled "Desenvolvimento de metodologia de exploração geológica para geodos de ametista e ágata, cobre e outros bens minerais em ambiente hidrotermal do Grupo Serra Geral, sul-sudeste do Brasil" and project of excellence from Programa de Apoio a Núcleos de Excelência (PRONEX), Fundação de Amparo à Pesquisa do Estado do Rio Grande do Sul (FAPERGS) and CNPq on strategic minerals from southern Brazil, coordinated by Léo A. Hartmann. The authors are grateful to Wilson Wildner and CPRM/PA (Geological Survey of Brazil) for the permission to use chemical analyses. AABC reviewer João Orestes S. Santos made a significant contribution to the quality of the article.

REFERENCES

AARNES I, SVENSEN H, CONNOLLY JAD AND PODLADCHICOV YY. 2010. How contact metamorphism can trigger global climate changes: Modeling gas generation around igneous sills in sedimentary basins. Geochim Cosmochim Ac 74: 7179-7195.

ABORRAGE AM AND LOPES RC. 1986. Projeto Borda Leste da Bacia do Paraná: integração geológica e avaliação econômica. DNPM/CPRM, São Paulo, final report, 18v.

ARAÚJO CC, YAMAMOTO JK AND ROSTIROLA SP. 2004. Distribuição espacial e caracterização geológica dos arenitos asfálticos da borda leste da Bacia do Paraná no Estado de São Paulo. Rev Bras Geocienc 34: 187-200.

ARIOLI EE. 2008. Arquitetura faciológica da sequência vulcânica e o significado exploratório das anomalias geoquímicas de elementos do grupo da platina (EGP) e metais associados no sistema magmático Serra Geral, Estado do Paraná, Brasil. PhD Thesis, Universidade Federal do Paraná, Curitiba, Brazil, 262 p.

BAKKER RJ. 2003. Package Fluids 1. Computer programs for analysis of fluid inclusion data and for modeling bulk fluid properties. Chem Geology 194: 3-23.

BRANDELIK A. 2009. CALCMIN – an EXCELTM Visual Basic application for calculating mineral structural formulae from electron microprobe analyses. Comput Geosci 35: 1540-1551.

BRÜCKMANN M, HARTMANN LA, KNIJNIK DB, ANDRADE RHP AND SATO K. 2013. Extended duration of Paraná volcanism 135-119 Ma. Annals, XIV Simpósio Nacional de Estudos Tectônicos, Chapada dos Guimarães. Mato Grosso, abstracts, 1 p.

CARON M, GOETHALS M, DE SCHMEDT G, BERGHMANS J, VLIEGEN S, VAN'T OOST E AND AARSSEN A. 1999. Pressure dependence of the auto-ignition temperature of methane/air mixtures. J Hazard Mater 65: 233-244.

CHEADLE MJ, ELLIOT MT AND MCKENZIE D. 2004. Percolation threshold and permeability of crystallizing igneous rocks: the importance of textural equilibrium. Geology 32: 757-760.

CORNWALL HR. 1951. Differentiation in lavas of the Keweenawan Series and the copper deposits of Michigan. Geol Soc Am Bull 62: 159-202.

COX KG, BELL JD AND PANKHURST RJ. 1979. The interpretation of igneous rocks. Allen and Unwin, London, 450 p.

CROCKET JH. 2002. Platinum-group element geochemistry of mafic and ultramafic rocks. In: Cabri LJ (Ed), The geology, geochemistry, mineralogy and mineral beneficiation of platinum-group elements: Ontario, Canada. Canadian Institute of Mining, Metallurgy and Petroleum 54: 177-210.

D'ORIANO C, POMPILIO M, BERTAGNINI A, CIONI R AND PICHAVANT M. 2013. Effects of experimental reheating of natural basaltic ash at different temperatures and redox conditions. Contrib Mineral Petrol 165: 863-883.

DRAGOVIC B AND PHILPOTTS A.R. 2002. Degree of crystal-mush compaction in the Holyoke basalt, CT, as inferred from overgrowths on plagioclase phenocrysts. Geological Society of America, 37th Annual Meeting.

DUARTE LC, HARTMANN LA, RONCHI LH, BERNER Z, THEYE T AND MASSONNE HJ. 2011. Stable isotope and mineralogical investigation of the genesis of amethyst geodes in the los Catalanes gemological district, Uruguai, southernmost Paraná volcanic province. Miner Deposita 46: 239-255.

DUARTE LC, HARTMANN LA, VASCONCELOS MAZ, MEDEIROS JTN AND THEYE T. 2009. Epigenetic formation of amethyst-bearing geodes from Los Catalanes gemological district, Artigas, Uruguay, southern Paraná Magmatic-Province. J Volcanol Geoth Res 184: 427-436.

FERREIRA CNH. 2011. Geologia do derrame Salto do Lontra e gênese dos pegmatitos básicos associados, província magmática do Paraná, sudoeste do estado do Paraná. Master of Science Dissertation (Unpublished). Universidade Federal do Paraná, Curitiba, Brazil, 102 p.

FERREIRA CNH, MESQUITA MJM, GOMES MEB, HILLEBRANDT P, VASCONCELLOS, EMG. 2014. Arquitetura interna e petrografia do derrame Salto do Lontra, sudoeste do estado do Paraná. Boletim Paranaense de Geociências 71-1: 46-59.

FODOR RV AND BAUER GR. 2014. Diabasic intrusion and lavas, segregation veins, and magma differentiation at Kahoolawe volcano, Hawaii. Miner Petrol 108: 269-286.

GOULART EP AND JARDIM NS. 1982. Avaliação geoquímica das Formações Ponta Grossa e Irati – Bacia do Paraná. In: Instituto de Pesquisas Tecnológicas do Estado de São Paulo (Ed), PauliPetro Consórcio CESP/IPT, p. 41-74.

GRAPES R. 2011. Pyrometamorphism. Springer-Verlag, Berlin, 365 p.

GRAPES R, SOKOL E, KOKH S, KOZMENKO O AND FISHMAN O. 2013. Petrogenesis of Na-rich paralava formed by methane flares associated with mud volcanism, Altyn-Emel National Park, Kazakhstan. Contrib Mineral Petr 165: 781-803.

GREENOUGH JD AND DOSTAL J. 1992a. Layered rhyolite bands in a tick North Mountain Basalt flow: the products of silicate liquid immiscibility? Mineral Mag 56:309-318.

GREENOUGH JD AND DOSTAL J. 1992b. Cooling history and differentiation of a thick North Mountain basalt flow (Nova Scotia, Canada). B Volcanol 55: 63-73.

GREENOUGH JD, LEE CY AND FRYER BJ. 2004. Evidence of volatile-influenced differentiation in a layered alkali

basalt flow, Penghu Islands, Taiwan. B Volcanol 60: 412-424.

HARTLEY ME AND THORDARSON T. 2009. Melt segregations in a Columbia River Basalt lava flow: A possible mechanism for the formation of highly evolved mafic magmas. Lithos 112: 434-446.

HARTMANN LA, BAGGIO SB AND DUARTE SK. 2013. Decoding geochemical and gamma-spectrometric signatures from lavas and sand injectites at the base of the Paraná volcanic province, Novo Hamburgo, Brazil. Int Geol Rev 55: 510-524.

HARTMANN LA ET AL. 2012a. Sequential opening and filling of cavities forming vesicles, amygdales and giant amethyst geodes in lavas from the southern Paraná volcanic province, Brazil and Uruguay. Int Geol Rev 54: 1-14.

HARTMANN LA, MEDEIROS JTN AND PETRUZZELLIS LT. 2012b. Numerical simulations of amethyst geode cavity formation by ballooning of altered Paraná volcanic rocks, South America. Geofluids 12: 133-141.

HOLZ M, FRANÇA AB, SOUZA PA, IANNUZZI R AND ROHN R. 2010. A stratigraphic chart of the Late Carboniferous/Permian succession of the eastern border of the Paraná Basin, Brazil, South America. J S Am Earth Sci 29: 381-399.

KONTAK DJ, DE WOLFE MY, YOUNG DE AND DOSTAL J. 2002. Late-stage crystallization history of the Jurassic North Mountain basalt, Nova Scotia, Canadá. I.Textural and chemical evidence for pervasive development of silicate-liquid immiscibility. Can Mineral 5: 1287-1311.

LARSEN RB, BROOKS CK AND BIRD D. 1992. Methane-bearing, aqueous, saline solutions in the Skaergaard intrusion, east Greenland. Contrib Mineral Petrol 112: 428-437.

MARIANI P, BRAITENBERG C AND USSAMI N. 2013. Explaining the thick crust in Paraná basin, Brazil, with satellite GOCE-gravity observations. J S Am Earth Sci 45: 209-223.

MARSH BD. 1995. Solidification fronts and magmatic evolution. Mineral Mag 60: 5-40.

MIDDLEMOST EAK. 1994. Naming materials in magma/igneous rock system. Earth Sci Rev 37: 215-224.

MORIMOTO N, FABRIES J, FERGUSON AK, GINZBURG IV, ROSS M, SEIFERT FA, ZUSSMAN J, AOKI K AND GOTTARDI G. 1988. Nomenclature of pyroxenes. Am Mineral 73: 1123-1133.

NAKAMURA K, SHIBUYA A, MASUTA K, MURAKAMI T, WILDNER W, DIAS AA, KIRCHNER CA AND LESSA N. 2003. Mineral exploration in the Paraná Basin area, the Federal Republic of Brazil, phase I. Metal Mining Agency of Japan - MMAJ and Geologycal Survey of Brazil - CPRM, internal report.

PEATE DW, HAWKESWORTH CJ AND MANTOVANI MSM. 1992. Chemical stratigraphy of the Paraná lavas (South America): classification of magma types and their spatial distribution. B Volcanol 55: 119-139.

PECK DL AND MINAKAMI T. 1968. The formation of columnar joints in the upper part of Kilauean lava lakes, Hawaii. Geol Soc Am Bull 79: 1151-1168.

PEREIRA R. 2013. Evolução da bacia do Paraná no Rio Grande do Sul. Master of Science Dissertation (Unpublished). Universidade do Estado do Rio de Janeiro, Rio de Janeiro, Brasil, www.fgel.uerj.br/prh17/renatapereiracsampaio_prh17_uerj_fgel_monografia.pdf (accessed february 26, 2014).

PHILPOTTS AR, BRUSTMAN CM, SHI J, CARLSON WD AND DENISON C. 1999. Plagioclase-chain networks in slowly cooled basaltic magma. Am Mineral 84: 1819-1829.

PHILPOTTS AR, CARROLL M AND HILL JM. 1996. Crystal-mush compaction and the origin of pegmatitic segregation sheets in a thick flood-basalt flow in the Mesozoic Hartford basin, Connecticut. J Petrol 37: 811-836.

PHILPOTTS AR AND DICKSON LD. 2002. Millimeter-scale modal layering and the nature of the upper solidification zone in thick flood-basalt flows and other sheets of magma. J Struct Geol 24: 1171-1177.

PUFFER JH AND HORTER DL. 1993. Origin of pegmatitic segregation veins within flood basalts. Geol Soc Am Bull 105: 738-748.

ROSENSTENGEL LM AND HARTMANN LA. 2012. Geochemical stratigraphy of lavas and fault-block structures in the Ametista do Sul geode mining district, Paraná volcanic province, southern Brazil. Ore Geol Rev 48: 332-348.

SAWAKUCHI AO, BELLO RM, NOMURA SF, OLIVEIRA AF, FERREIRA MP, FUZIKAWA K, SAYEG IJ AND GIANNINI PCF. 2011. Paleotermometria das unidades permotriássicas da borda leste da Bacia do Paraná (SP). Annals, XIII Simpósio Nacional de Estudos Tectônicos, Campinas, São Paulo, 4 p.

SCHENATO F, FORMOSO M, DUDOIGNON P, MEUNIER A, PROUST D AND MAS A. 2003. Alteration processes of a thick basaltic lava flow of the Paraná Basin (Brazil): petrographic and mineralogical studies. J S Am Earth Sci 16: 423-444.

SILVA KFB. 2011. Caracterização petrográfica e geoquímica de pegmatitos básicos, encaixados em derrames basálticos do Grupo Serra Geral, no Estado do Paraná. Course conclusion monograph. Universidade Estadual de Campinas, Campinas, Brazil, 94 p.

SIMAS MW, GUERRA-SOMMER M, CAZZULO-KLEPZIG M, MENEGAT R, SANTOS JOS, FERREIRA JAF AND DEGANI-SCHMIDT I. 2012. Geochronological correlation of the main coal interval in Brazilian Lower Permian: Radiometric dating of tonstein and calibration of biostratigraphic framework. J S Am Earth Sci 39: 1-15.

SOKOL E, NOVIKOV I, ZATEEVA S, VAPNIK YE, SHAGAM R AND KOZMENKO O. 2010. Combustion metamorphism in the Nabi Musa dome: for a mud volcanic origin of the Mottled Zone, Dead Sea area. Basin Res 22: 414-438.

STEELE-MACINNIS M, BODNAR RJ AND NADEN J. 2011. Numerical model to determine the composition of H_2O–NaCl–$CaCl_2$ fluid inclusions based on microthermometric and microanalytical data. Geochim Cosmochim Ac 75:21-40.

VASCONCELLOS EMG, LICHT OAB, BRAGA LS AND BITTENCOURT AVL. 2001. Gabros da Bacia do Paraná: aspectos petrográficos e geoquímicos. Annals, VIII Congresso Brasileiro de Geoquímica, Curitiba, Paraná, abstracts, 1 p.

WALKER F. 1953. The pegmatitic differentiates of basic sheets. Am J Sci 251: 41-60.

WILDNER W, ARIOLI EE, LICHT OAB, COSTA VS, CARRILHO JC, LONGO EG, CANTARINO SC, SANDER A, PERROTA M AND FILHO CRS. 2006. Geologia e Recursos Minerais do Sudoeste do Estado do Paraná. Convênio CPRM/ MINEROPAR, Brasília, Distrito Federal, 95 p.